Siege of the South: Hunga Tonga-Hunga Ha'apai Water Vapor Excluded from 2022 Antarctic Stratospheric Polar Vortex

Gloria L Manney[1], Michelle L. Santee[2], Alyn Lambert[3], Luis Millan[4], Ken Minschwaner[5], Frank Werner[2], Zachary Duane Lawrence[6], William G. Read[3], Nathaniel J Livesey[2], and Tao Wang[7]

[1]Northwest Research Associates
[2]Jet Propulsion Laboratory
[3]Jet Propulsion Lab (NASA)
[4]Jet propulsion laboratory
[5]New Mexico Institute of Mining and Technology
[6]CIRES/NOAA
[7]NASA JPL / Caltech

April 4, 2023

Abstract

We use Aura Microwave Limb Sounder (MLS) trace gas measurements to investigate whether water vapor (H2O) injected into the stratosphere by the Hunga Tonga-Hunga Ha'apai (HTHH) eruption affected the 2022 Antarctic stratospheric vortex. Other MLS-measured long-lived species are used to distinguish high HTHH H2O from that descending in the vortex from the upper-stratospheric H2O peak. HTHH H2O reached high southern latitudes in June–July but was effectively excluded from the vortex by the strong transport barrier at its edge. MLS H2O, nitric acid, chlorine species, and ozone within the 2022 Antarctic polar vortex were near average; the vortex was large, strong, and long-lived, but not exceptionally so. There is thus no clear evidence of HTHH influence on the 2022 Antarctic vortex or its composition. Substantial impacts on the stratospheric polar vortices are expected in succeeding years since the H2O injected by HTHH has spread globally.

Siege of the South: Hunga Tonga-Hunga Ha'apai Water Vapor Excluded from 2022 Antarctic Stratospheric Polar Vortex

Gloria L. Manney[1,2], Michelle L. Santee[3], Alyn Lambert[3], Luis F. Millán[3], Ken Minschwaner[2], Frank Werner[3], Zachary D. Lawrence[4,5], William G. Read[3], Nathaniel J. Livesey[3], Tao Wang[3]

[1]NorthWest Research Associates, Socorro, NM, USA
[2]New Mexico Institute of Mining and Technology, Socorro, NM, USA
[3]Jet Propulsion Laboratory, California Institute of Technology, Pasadena, CA, USA
[4]Cooperative Institute for Research in Environmental Sciences (CIRES) & NOAA Physical Sciences Laboratory (PSL), University of Colorado, Boulder, Colorado, USA.
[5]NorthWest Research Associates, Boulder, CO, USA

Key Points:

- MLS trace gas data show that the Hunga Tonga-Hunga Ha'apai H_2O plume was effectively excluded from the 2022 Antarctic polar vortex
- Antarctic lower stratospheric vortex strength, size, and longevity were among the largest on record, but within the range of previous years
- Antarctic chemical ozone loss in 2022 was unexceptional, with MLS ozone and related trace gases observed to be near average

Corresponding author: Gloria L Manney, `manney@nwra.com`

Abstract

We use Aura Microwave Limb Sounder (MLS) trace gas measurements to investigate whether water vapor (H_2O) injected into the stratosphere by the Hunga Tonga-Hunga Ha'apai (HTHH) eruption affected the 2022 Antarctic stratospheric vortex. Other MLS-measured long-lived species are used to distinguish high HTHH H_2O from that descending in the vortex from the upper-stratospheric H_2O peak. HTHH H_2O reached high southern latitudes in June–July but was effectively excluded from the vortex by the strong transport barrier at its edge. MLS H_2O, nitric acid, chlorine species, and ozone within the 2022 Antarctic polar vortex were near average; the vortex was large, strong, and long-lived, but not exceptionally so. There is thus no clear evidence of HTHH influence on the 2022 Antarctic vortex or its composition. Substantial impacts on the stratospheric polar vortices are expected in succeeding years since the H_2O injected by HTHH has spread globally.

Plain Language Summary

The 2022 Hunga Tonga-Hunga Ha'apai eruption injected vast amounts of water vapor into the stratosphere. There has been much speculation that this large increase in water vapor could impact the Antarctic stratospheric polar vortex and Antarctic ozone hole: Water vapor plays an important role in polar vortex ozone depletion by providing the necessary conditions for the formation of polar stratospheric clouds. These clouds provide surfaces on which ozone-depleting chemical reactions can occur. The excess water vapor could also change the vortex evolution via water vapor's effects on temperature, which could in turn affect the strong band of winds demarking the polar vortex edge. We use satellite measurements of water vapor and other gasses to show that by the time the water vapor from the Hunga Tonga volcanic eruption reached the south polar regions in June–July 2022, the polar vortex was too strong for it to penetrate. Measurements of water vapor, ozone, and chemicals involved in destroying ozone all showed near-average amounts and evolution within the vortex. In future years, larger effects on the polar vortex and chemical processing are expected because water vapor from Hunga Tonga that has spread globally will be entrained into the polar vortex.

1 Introduction

The 15 January 2022 eruption of the underwater volcano Hunga Tonga-Hunga Ha'apai (HTHH) injected an unprecedented amount of water vapor (H_2O) directly into the stratosphere, increasing the stratospheric H_2O burden by approximately 10% (e.g., Millán et al., 2022; Vömel et al., 2022). It also resulted in substantial, though not unprecedented, enhancements in volcanic aerosol loading (Khaykin et al., 2022; Sellitto et al., 2022; Taha et al., 2022). Numerous studies have already explored aspects of the stratospheric impacts of HTHH enhancements in aerosol and H_2O; of particular relevance here are suggestions that H_2O and aerosol from HTHH injected into the Southern Hemisphere (SH) stratosphere took many months to reach high latitudes and did not extend poleward of about 60°S (e.g., Legras et al., 2022; Khaykin et al., 2022; Schoeberl et al., 2022; Zhu et al., 2022). In the lowermost stratosphere (at and below approximately the 380 K isentropic surface), a few studies suggest that some H_2O and aerosol were transported to high SH latitudes within days to weeks via the shallow branch of the Brewer-Dobson circulation (e.g. Taha et al., 2022; Schoeberl et al., 2022; Khaykin et al., 2022). Radiative cooling from HTHH H_2O led to unprecedented cold in SH mid/low latitudes, with associated circulation and transport anomalies (Coy et al., 2022; Schoeberl et al., 2022; Sellitto et al., 2022).

It was suggested that transport of HTHH aerosol and H_2O into high SH latitudes might impact the composition of the 2022 SH stratospheric polar vortex, and that circulation changes associated with the HTHH H_2O plume might affect the strength, size, and / or longevity of that vortex (e.g., Taha et al., 2022; Zhu et al., 2022). Here we use Aura Microwave Limb Sounder (MLS) data to analyze the evolution of the SH stratospheric polar vortex in 2022, transport of the HTHH H_2O plume in relation to it, and chemical processing within it. We find no evidence of substantial impacts of HTHH on the 2022 SH polar vortex or the chemical processing and ozone loss within it. We use temperature, H_2O, N_2O, CO, HCl, ClO, and O_3 from v5 MLS "level 3" (L3) data (Livesey et al., 2020), along with meteorological fields from NASA's Modern Era Retrospective-analysis for Research and Applications Version 2 (MERRA-2) dataset (Gelaro et al., 2017; Global Modeling and Assimilation Office (GMAO), 2015).

Immediately following the eruption, standard MLS v5 quality screening (Livesey et al., 2020) flagged many of the profiles most affected by HTHH as suspect retrievals (Millán et al., 2022); thus the H_2O, N_2O, and HNO_3 anomalies shown here may be artificially small for up to three weeks after the eruption. Since our focus is on the subsequent transport and relationship to the SH polar vortex, our results are unaffected.

2 Transport of HTHH Stratospheric H_2O

Figure 1 shows the evolution of N_2O and H_2O (both generally long-lived tracers of transport in the stratosphere) anomalies in the SH lower through middle stratosphere, in vortex averages as a function of height (expressed as potential temperature, θ) and as a function of equivalent latitude (EqL, the latitude enclosing the same area between it and the pole as a given potential vorticity, PV, contour, Butchart & Remsberg, 1986) on several isentropic (θ) surfaces. The past five years include seasons with exceptionally warm / short-lived (2019) and cold / long-lived (2020 and 2021) springtime polar vortices, as well as a year (2018) with more typical vortex characteristics (WMO, 2023). (Figs. S1–S2 in the Supporting Information, SI, show the full-mission and include MLS temperature.) The evolution of vortex-average N_2O (Fig. 1a) in 2022 is unexceptional, showing positive anomalies except at the lowest levels; such a vertical dipole pattern of N_2O anomalies is common, with primarily higher values in 2020, 2021, and 2022 consistent with lower vortex temperatures (see below and Figs. S1–3) and accompanying weaker diabatic descent (Fig. S4). N_2O EqL/time evolution (Fig. 1b–f) is also fairly typical; recurring changes above 430 K from high to low anomalies extending from low latitudes show quasi-biennial oscillation (QBO) related transport (e.g.. Baldwin et al., 2001; Diallo et al., 2019). Low N_2O anomalies in austral spring 2020 and 2021 are related to the delayed vortex breakup in those years, with low N_2O values remaining confined longer in a more persistent vortex. Spring 2022 shows similar, but weaker, anomalies, suggesting a long-lived vortex. In contrast, high anomalies in 2019 result from a rare SH sudden stratospheric warming that led to a small, warm, and short-lived vortex (e.g., Wargan et al., 2020).

H_2O anomalies (Fig. 1g–l) in the SH lower stratospheric vortex are typically dominated by interannual variations in polar stratospheric cloud extent; strong low H_2O anomalies in spring 2020 and 2021 at 500 K and surrounding levels arose from persistent cold anomalies in unusually long-lasting vortices. Outside the vortex (Fig. 1h–lFig. 1g–l), high H_2O anomalies often accompany low N_2O anomalies because H_2O and N_2O have opposite vertical and horizontal gradients in the lower to middle stratosphere. For example, low (high) springtime H_2O (N_2O) anomalies just outside the vortex edge in 2019, and opposite patterns in 2020 and 2021 at 600–850 K; similar patterns are seen in mid-Eqls in earlier years (Fig. S1). (Note that typical H_2O anomalies prior to 2022 are washed out by the large colorbar range needed to portray the HTHH H_2O.) Above 500 K, typical signatures of extra-vortex transport of H_2O are overwhelmed by the arrival of HTHH H_2O (Fig. 1h–j, Fig. S1). HTHH H_2O reached the vortex edge in early June 2022, after the vortex was fully developed except in the lowermost stratosphere. Above 500 K, extremely strong gradients along the vortex edge suggest that the HTHH plume could not penetrate the vortex edge. Pervasive high H_2O anomalies since early 2020 below about 500 K may reflect lingering enhancements from the 2020 Australian New Years fires (e.g., Santee et al., 2022). While small positive anomalies encroach into the vortex region in late winter 2022 at 500 K (near the lowest altitude of large HTHH enhancement) and 430 K, similar features are common (e.g., in 2018 and 2021), so it is unclear whether they are related to the HTHH plume. At all levels examined (including the lowermost stratosphere, e.g., Fig. S3), H_2O anomalies inside the vortex are within the typical range.

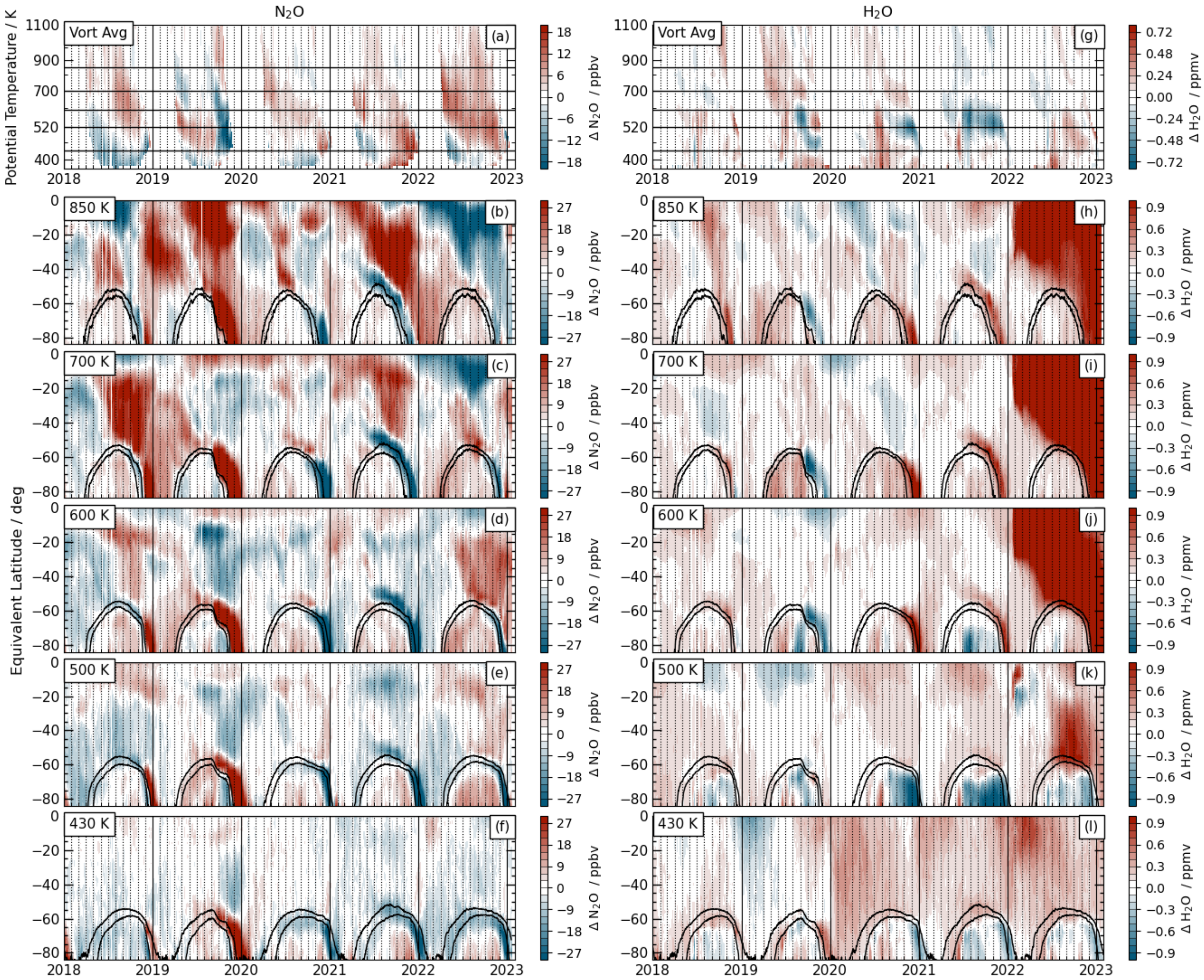

Figure 1. Evolution of MLS-observed SH anomalies from the baseline 2005–2021 climatology of N_2O (a–f) and H_2O (g–l) from January 2018 through January 2023: (a,g) vortex-averaged values; (b–f, h–l) evolution as a function of EqL at levels in the middle through lower stratosphere (horizontal lines in a,g). Black contours in b–f and h–l are sPV values indicating the vortex edge region.

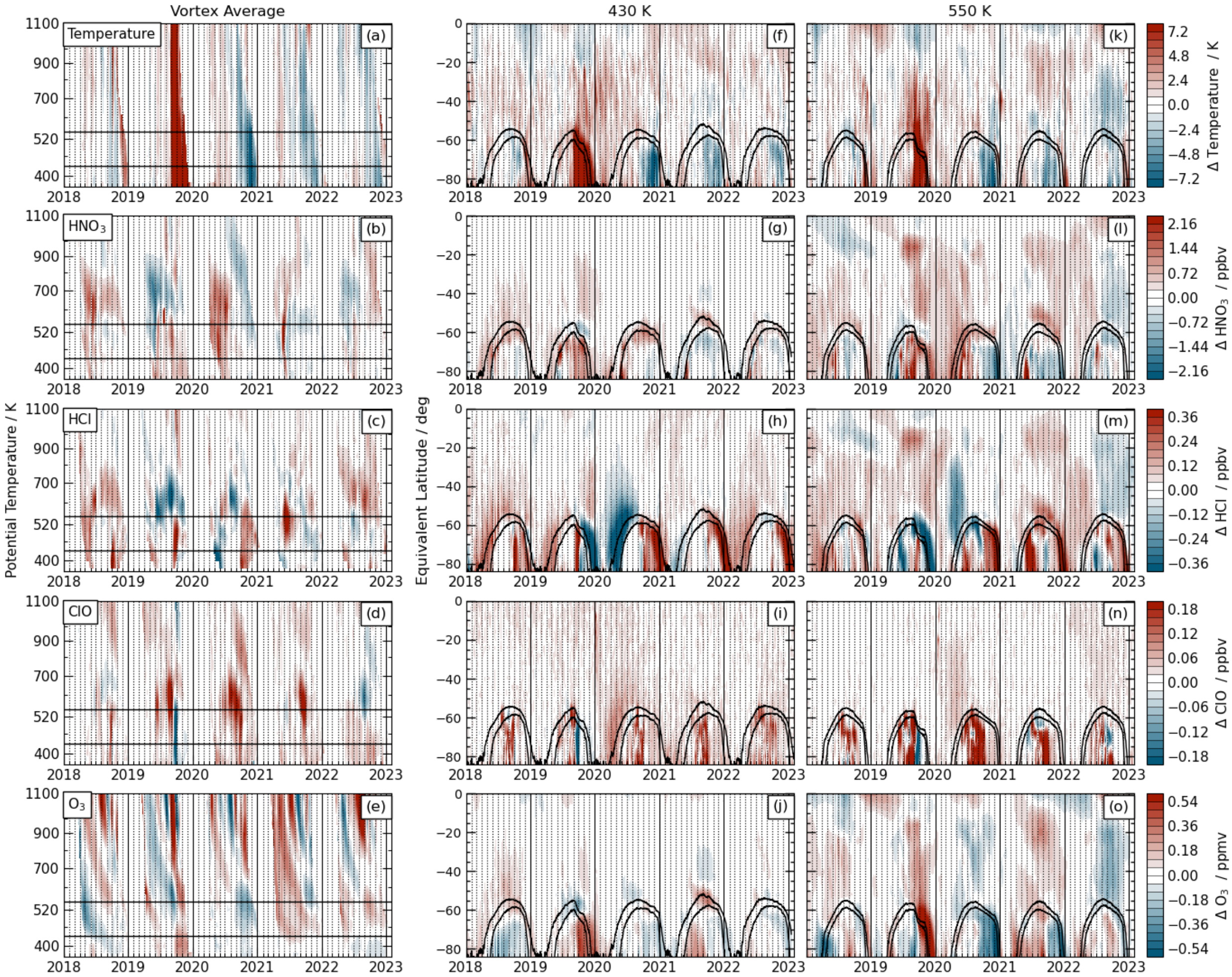

Figure 2. As in Fig. 1, but for MLS temperature, HNO_3, HCl, ClO, and O_3; (a–e) vortex averages, (f–j) 430 K, and (k–o) 550 K EqL timeseries, for January 2018 through January 2023. Black contours (f–o) are sPV values demarking the vortex edge region.

3 Polar Vortex Composition and Chemical Processing

Figure 2 shows a similar view of MLS measurements of temperature and species involved in polar chemical processing (Figs. S1–3 show 550 K, 430 K, and 380 K for the full mission). The Antarctic vortex was unusually cold and persistent in spring 2022, but less so than in 2020 and 2021. Vortex HNO_3 values were near average throughout the season. Vortex HCl and ClO commonly oscillate between high and low anomalies, and thus they are also generally unexceptional within the 2022 vortex; the high HCl anomalies in spring are related primarily to longer-than-usual confinement of the very high values that ensue from chlorine deactivation. Consistent with near-average vortex values of chlorine species, O_3 anomalies in 2022 were also relatively small. Both 2020 and 2021 showed lower O_3, consistent with larger cold anomalies and even longer-lived (see below) vortices in those years than in 2022. Outside the vortex, temperature anomalies (arising from radiative effects of HTHH H_2O, e.g., Coy et al., 2022; Schoeberl et al., 2022) and associated mid-latitude transport anomalies (Coy et al., 2022) appear consistent with the extravortex high N_2O anomalies seen near 500–600 K (Fig. 1), and suggest that accompanying extravortex HCl, HNO_3, and O_3 anomalies are at least partially transport-driven.

Figure 3 provides a closer look at the EqL/θ evolution of MLS trace gases in 2022, showing snapshots of anomalies from climatology (similar anomaly plots in 2018, 2020, and 2021 are shown in Figs. S5–S7). The H_2O plume first approached the SH polar vortex edge in early to mid-June. Subsequently, extremely strong H_2O gradients developed along the vortex edge over 520–800 K and persisted through October (into December below about 700 K; see also Fig 1). By mid-December, only a weak remnant of the vortex remained below about 520 K, and the H_2O enhancement extended into high latitudes above that level. MLS data show no indication of air from the HTHH H_2O plume penetrating substantially into the SH vortex before its breakup. N_2O anomalies within the vortex were generally small until austral spring; below about 700 K, these anomalies were near zero from August through October. Low N_2O anomalies along the vortex edge beginning in early November are consistent with confinement in an unusually persistent vortex. Mid-latitude cold anomalies throughout the middle stratosphere (e.g., Coy et al., 2022; Schoeberl et al., 2022) are apparent from June through mid-December. Vortex temperatures were below average through much of the season, with largest cold anomalies in October and November (also see Fig. 2). High extra-vortex N_2O anomalies through this period are consistent in extent and location with the circulation anomalies reported by Coy et al. (2022). The co-location of N_2O anomalies with those in HNO_3, HCl, and O_3 suggests that transport plays a role in all of them; work is in progress analyzing the relative effects of dynamical and chemical processes.

Within the vortex, HNO_3 is slightly lower than usual, consistent with a colder-than-average vortex. HCl (ClO) shows low (high) anomalies during much (but not all, e.g., Fig. 3A,G) of the winter. As noted above, high HCl anomalies appear along the vortex edge in November and in the vortex remnant in mid-December, consistent with high values resulting from deactivation into HCl (as is typical in the SH, e.g., Santee et al., 2008) followed by unusually enduring confinement in the persistent vortex. Lower stratospheric O_3 anomalies in the early winter (before extensive chemical loss) are slightly positive and remain so through October (e.g., Fig. 3O). Taken together, the results in Figs. 2 and 3 suggest that the modest low anomalies in O_3 seen in austral spring 2022 (e.g., Fig. 3P) result primarily (if not entirely) from the unusual persistence of the vortex.

4 Vortex Evolution and Trace Gas Confinement

Figure 4 summarizes the evolution of the 2022 SH vortex in the context of the 43-year MERRA-2 record and the evolution of trace gases in the context of the 18-year MLS record, both in relation to the previous three SH winters. Figure S8 shows profiles of additional MERRA-2 diagnostics of vortex strength and longevity. Consistent with the indications in the trace gases of its unusual persistence, the 2022 SH late winter and spring vortex was among the largest on record at levels up to about 650 K, approximately matching the maximum size and persistence seen prior to 2020 (Fig. 4a–d; Fig. S8b,d). In spring, the 2021 vortex area was slightly larger, and the 2020 vortex area substantially larger than that in 2022 from about 460 K to 650 K, with 2020 setting the record for lower-stratospheric vortex persistence (Fig. 4a–c, S8b–d). Maximum PV gradients, indicating vortex strength (that is, robustness as a transport barrier), show unusually strong springtime vortices in 2020 through 2022 below about 500 K, but only the 2020 vortex was stronger than average above about 600 K (Fig. 4e–h; Fig. S8a). Below about 520 K, the area with temperatures below the nitric acid trihydrate (NAT) and ice polar stratospheric cloud (PSC) thresholds was larger than usual (Fig 4m,n,q,r) and PSCs persisted later than usual (Fig. 4m–t, Fig. S8e,f) in spring 2020, 2021, and 2022, but only exceeded previous springtime records in 2020; above about 600 K PSC area and duration were near average.

The unexceptional MLS trace gas evolution in the 2022 Antarctic vortex is highlighted in Fig. 4A–P (Fig. S9 shows the vertical structure). Interannual variability in SH polar chemical processing is relatively small, but, with few exceptions, all of the trace gases show 2022 evolution that is well within the previously observed range. Over ∼450–600 K, persistently low H_2O after October in 2022, and to an even greater extent in 2020 and 2021, is consistent with confinement of dehydrated air in long-lived vortices. Chlorine evolution (seen in HCl and ClO, Fig. 4E–

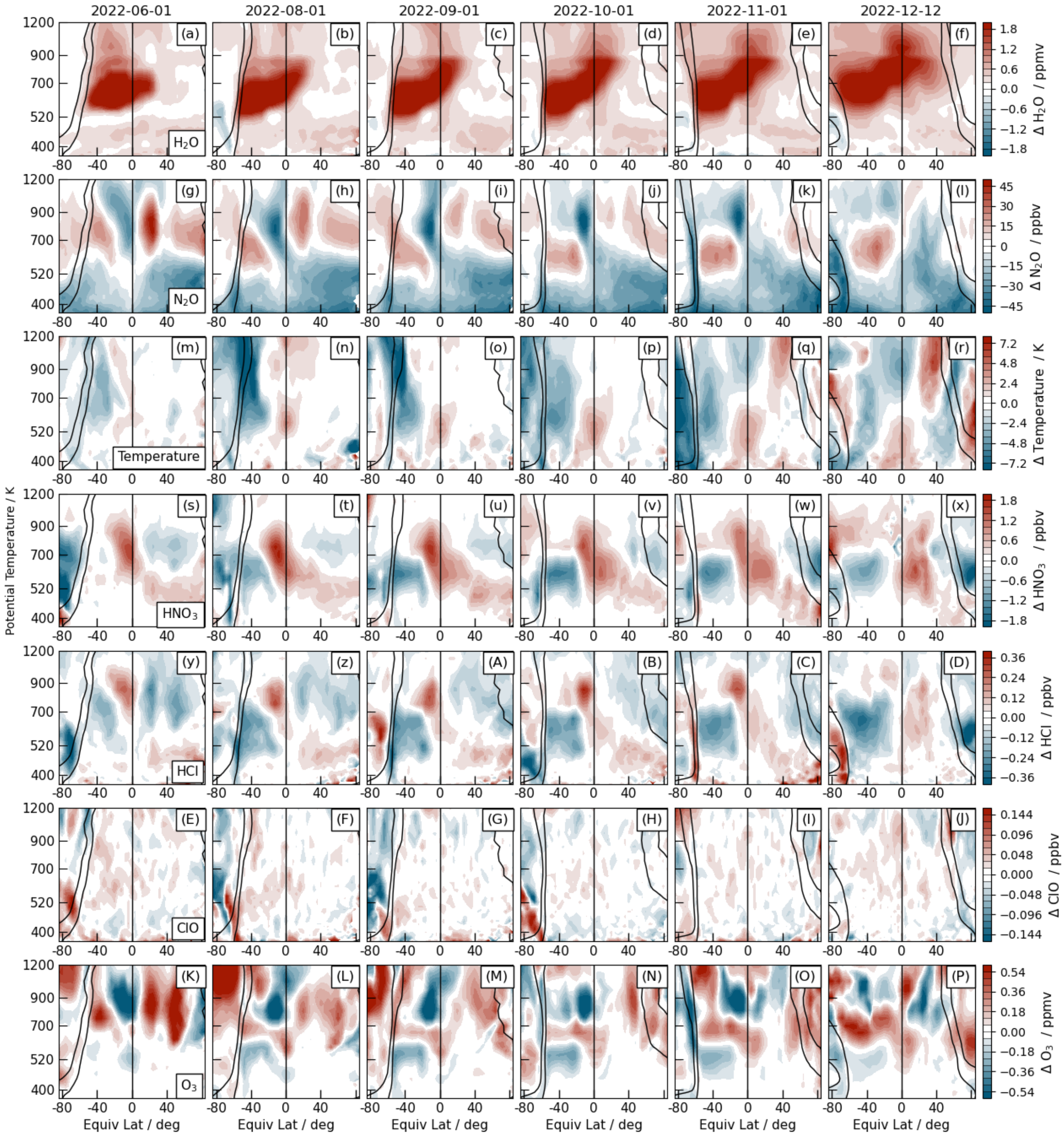

Figure 3. Snapshots on selected days in 2022 of anomalies from the baseline 2005–2021 climatology of MLS (a–f) H_2O, (g–l) N_2O, (m–r) temperature, (s–x) HNO_3, (y–D) HCl, (E–J) ClO, and (K–P) O_3. Black contours show sPV values demarking the vortex edge region.

L; Fig. S9q–x) was fairly typical throughout the season. Observed O_3 evolution in 2022 was remarkably near average throughout the season (Fig. 4M–P; Fig. S9y–B).

The above results provide visual evidence that the vortex edge presented an effective transport barrier, preventing substantial penetration of the HTHH H_2O plume. To look more closely at the robustness of the vortex edge transport barrier, Fig. 5 shows scatter and density plots of H_2O versus N_2O and sPV for representative days in 2022 compared with the evolution in all prior years in the MLS record. Low N_2O (relative to the range of values at a given level) and high-magnitude sPV identify vortex air parcels. In the lower stratosphere (exemplified by 550 K), increasingly low vortex H_2O through the season results from dehydration and is very similar to that previously observed by MLS (density plots, right columns, emphasize the similarity of the main distributions in 2022 to those in earlier years). Extravortex H_2O at 550 K does not stand out from the previous record before July, but after that the HTHH enhancement manifests as a distinct cluster of high H_2O with N_2O near 200 ppbv and sPV magnitudes $<1\times10^{-4}$ s^{-1} (both values that are unambiguously extravortex) that is unique to 2022 (compare yellow-orange / purple H_2O / sPV values with grey dots; orange with grey contours). In the middle stratosphere (exemplified by 700 K), vortex H_2O values first increase via descent of the upper stratospheric peak, then decrease as continuing descent brings low mesospheric H_2O into the stratospheric vortex (e.g., Ray et al., 2002; Lee et al., 2011); both the high (e.g., Fig. 5a–d) and the low (e.g., Fig. 5e–l) H_2O values that descend through the vortex (low N_2O, high-magnitude sPV end of the x-axis) at 700 K are distinct from the extravortex population of high H_2O from HTHH, and that is in turn distinguished from extravortex air in previous years by higher H_2O values at extravortex N_2O ($\sim$150–200 ppbv) and sPV (magnitude $<\sim1\times10^{-4}$ s^{-1}). These correlations of H_2O with N_2O and sPV (especially the density plots versus sPV) show clearly that the air with enhanced H_2O from HTHH remained well separated from that within the vortex until vortex breakup at each level (as suggested in Figs. 1 and 3). MLS H_2O / CO correlations show a similar picture in the middle (Fig. S10) and upper stratosphere, with HTHH H_2O associated with low CO values characteristic of extravortex air. Further, because the seawater from HTHH has a higher ratio of HDO to H_2O than background water vapor in the extravortex stratosphere (e.g., Randel et al., 2012; Khaykin et al., 2022), an unprecedented increase in that ratio in SH midlatitudes also marks the HTHH air as separate from (and excluded from) that in the vortex (Figs. S11–12).

5 Summary

The unprecedented water vapor injection into the stratosphere by HTHH is tracked using MLS and reanalysis data. The H_2O plume [[or The enhanced H_2O]] is shown to have been effectively excluded from the 2022 Antarctic polar vortex until the vortex breakdown. In contrast to speculation that HTHH stratospheric H_2O and aerosol injections would lead to substantial anomalies in the Antarctic polar vortex and lower stratospheric polar processing and ozone loss within it (e.g., Taha et al., 2022; Zhu et al., 2022), our analysis suggests that HTHH did not cause substantial changes in polar processing and ozone loss within the vortex: MLS observations of HNO_3, HCl, ClO, and O_3 inside the vortex through the depth of the lower stratosphere all show evolution well within the range of previous years during the MLS mission, with near-average O_3 loss. Evidence for possible dynamical impacts on the vortex is likewise not unequivocal: The vortex was among the larger, stronger, and longer-lived in the SH lower stratosphere, but these conditions were matched or exceeded by those in 2020, 2021, and several previous years in the MERRA-2 record since 1980; vortex cold anomalies were even less exceptional. Thus, despite large radiative, dynamical, and composition perturbations in midlatitudes, the observational evidence shows that chemical processing within the 2022 Antarctic stratospheric polar vortex was fairly typical, and does not show clear evidence of substantial dynamical vortex perturbations. The dispersal of HTHH H_2O following the Antarctic vortex breakup (e.g., Fig. 1) led to unprecedented high H_2O anomalies throughout the SH, which are expected to linger for at least several years (e.g., Millán et al., 2022; Khaykin et al., 2022), raising the expectation of large perturbations to Antarctic polar vortex chemistry and the ozone hole in 2023 and beyond. HTHH H_2O has also been transported into the Northern Hemisphere (e.g., Schoeberl et al., 2023), but reached the Arctic vor-

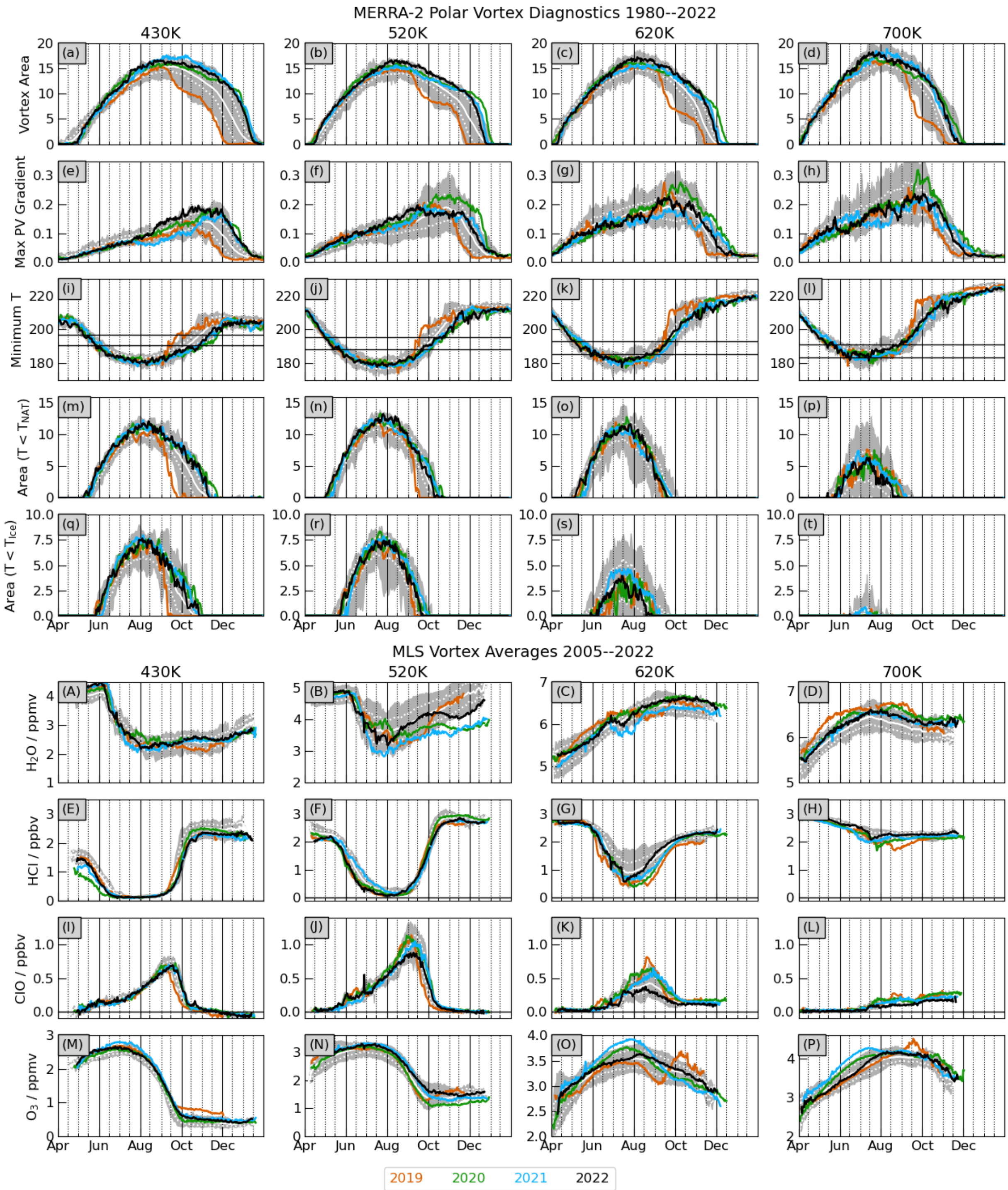

Figure 4. (a–t) Time series at four levels in the lower to middle stratosphere of vortex area, maximum PV gradients, high latitude (poleward of 30°) minimum temperature, and area below NAT and ice PSC thresholds, comparing 2019 (orange), 2020 (green), 2021 (cyan), and 2022 (black) with the range (shading), mean (solid white line), and one standard deviation envelope (dotted white lines) over 1980–2018. (A–P) Vortex-averaged H_2O, HCl, ClO, and O_3 in same format as for the dynamical fields, with the range over 2005–2018.

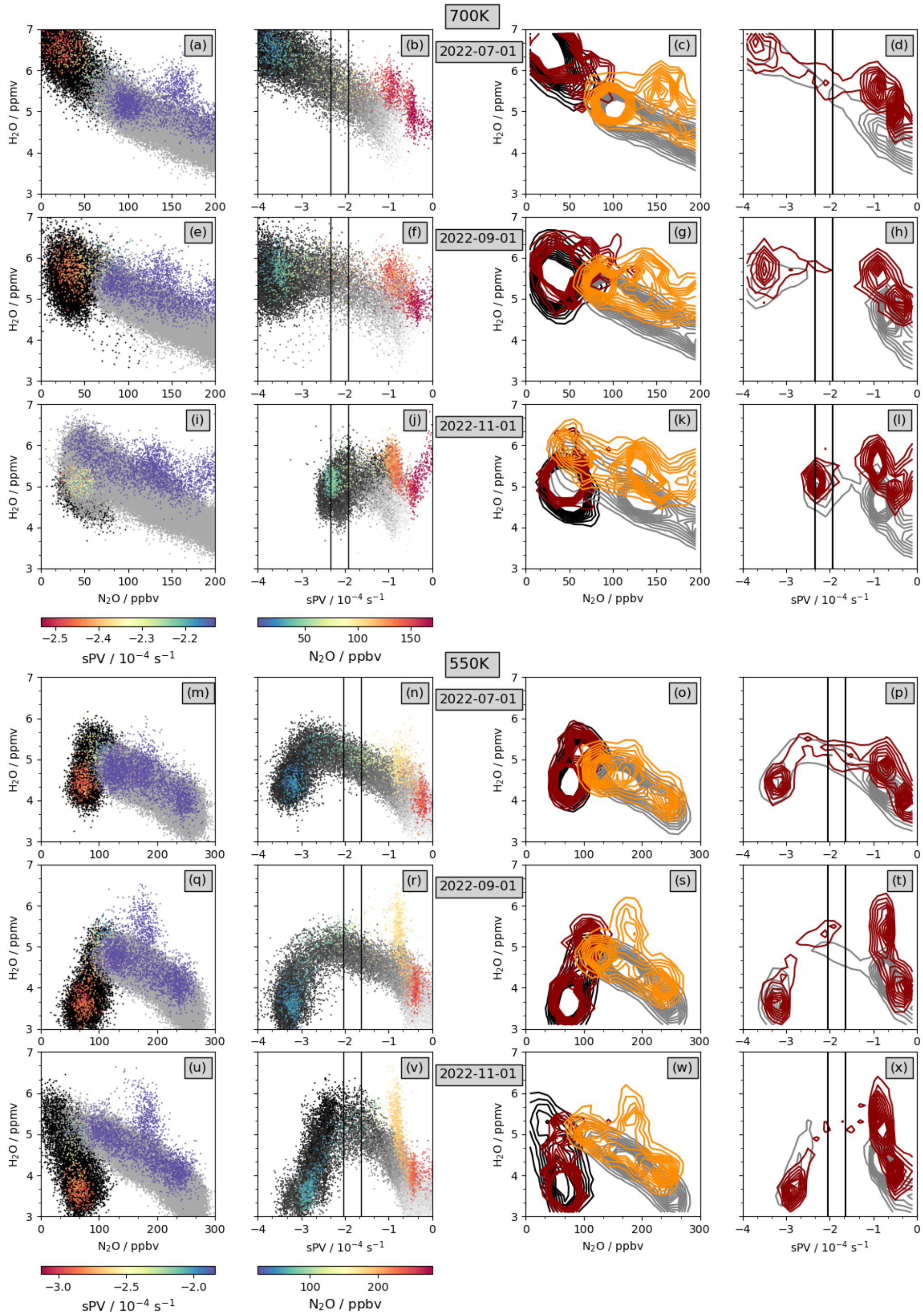

Figure 5. Scatter (left two columns) and density (right two columns) plots of MLS H_2O (y-axis) versus N_2O (first and third columns) and sPV (second and last columns). Grey and black dots (contours) show values from 2005–2021 in the scatter (density) plots; for those years, black (grey) indicates x-axis values of N_2O or sPV characteristic of inside (outside) the vortex. For 2022, colored (purple) dots or dark red (orange) contours show sPV values inside (outside) the vortex. 2022 N_2O (second column) is colored such that blue/blue-green shows typical vortex values. Black vertical lines on the plots versus sPV indicate the vortex edge region.

tex edge after the vortex was well-developed and was only dispersed through the NH after a strong sudden stratospheric warming starting in mid-February (paper in preparation). Thus large effects on Arctic polar vortex chemistry are also expected to manifest starting in the 2023/2024 cool season.

6 Open Research

The data used herein are publicly available as follows:

- MERRA-2: (Global Modeling and Assimilation Office (GMAO), 2015) `https://disc.sci.gsfc.nasa.gov/uui/datasets?keywords=%22MERRA-2%22`
- Aura MLS Level-2 and Level-3 data: (Lambert, Read, & Livesey, 2020; Lambert, Livesey, & Read, 2020; Lambert et al., 2021b, 2021a; Schwartz, Pumphrey, et al., 2020; Schwartz, Froidevaux, et al., 2020; Schwartz, Pumphrey, et al., 2021; Schwartz, Froidevaux, et al., 2021) `https://disc.gsfc.nasa.gov/datasets?page=1&keywords=AURA%20MLS`
- ACE-FTS v4.1/4.2 data: `http://www.ace.uwaterloo.ca` (registration required)
- ACE-FTS v4.1/4.2 error flags: `https://dataverse.scholarsportal.info/api/access/dataset/:persistentId/versions/:latest?persistentId=doi:10.5683/SP2/BC4ATC`
- MLS & ACE-FTS derived meteorological products: `https://mls.jpl.nasa.gov/eos-aura-mls/dmp` (registration required).

Acknowledgments

Thanks to the MLS team at JPL for data processing and analysis support, especially Brian Knosp for data management, Ryan Fuller for development and production of the MLS L3 products, and Lucien Froidevaux and Michael Schwartz for helpful discussions. Thanks to the ACE science team for making the ACE-FTS data available, especially Kaley Walker and Patrick Sheese for advice on data quality and usage. Thanks to the GMAO for providing the MERRA-2 dataset. G.L. Manney was supported by the Jet Propulsion Laboratory (JPL) Microwave Limb Sounder team under JPL subcontract #1521127 to NWRA. Work at the Jet Propulsion Laboratory, California Institute of Technology, was carried out under a contract with the National Aeronautics and Space Administration (80NM0018D0004).

References

Baldwin, M. P., Gray, L. J., Dunkerton, T. J., Hamilton, K., Haynes, P. H., J, W., ... Takahasi, M. (2001). The quasi-biennial oscillation. *Rev. Geophys.*, *39*, 179–229.

Boone, C., Bernath, P., Cok, D., Jones, S., & Steffen, J. (2020). Version 4 retrievals for the atmospheric chemistry experiment Fourier transform spectrometer (ACE-FTS) and imagers. *Journal of Quantitative Spectroscopy and Radiative Transfer*, *247*, 106939. Retrieved from `https://www.sciencedirect.com/science/article/pii/S0022407319305916` doi: https://doi.org/10.1016/j.jqsrt.2020.106939

Butchart, N., & Remsberg, E. E. (1986). The area of the stratospheric polar vortex as a diagnostic for tracer transport on an isentropic surface. *J. Atmos. Sci.*, *43*, 1319–1339.

Coy, L., Newman, P. A., Wargan, K., Partyka, G., Strahan, S. E., & Pawson, S. (2022). Stratospheric Circulation Changes Associated With the Hunga Tonga-Hunga Ha'apai Eruption. *Geophysical Research Letters*, *49*(22), e2022GL100982. Retrieved 2022-11-27, from `https://onlinelibrary.wiley.com/doi/abs/10.1029/2022GL100982` (_eprint: https://onlinelibrary.wiley.com/doi/pdf/10.1029/2022GL100982) doi: 10.1029/2022GL100982

Diallo, M., Konopka, P., Santee, M. L., Müller, R., Tao, M., Walker, K. A., ... Ploeger,

F. (2019). Structural changes in the shallow and transition branch of the Brewer–Dobson circulation induced by El Niño. *Atmos. Chem. Phys.*, *19*(1), 425–446. Retrieved from https://acp.copernicus.org/articles/19/425/2019/ doi: 10.5194/acp-19-425-2019

Gelaro, R., McCarty, W., Suárez, M. J., Todling, R., Molod, A., Takacs, L., … Zhao, B. (2017). The Modern-Era Retrospective Analysis for Research and Applications, Version-2 (MERRA-2). *J. Clim.*, *30*, 5419–5454. doi: doi:10.1175/JCLI-D-16-0758.1

Global Modeling and Assimilation Office (GMAO). (2015). *MERRA-2 inst3_3d_asm_nv: 3d, 3-hourly,instantaneous, model-level, assimilation, assimilated meteorological fields v5.12.4, Greenbelt, MD, USA, Goddard Earth Sciences Data and Information Services Center (GES DISC), accessed 1 June 2022* [dataset]. doi: 10.5067/WWQSXQ8IVFW8

Khaykin, S., Podglajen, A., Ploeger, F., Grooß, J.-U., Tence, F., Bekki, S., … Ravetta, F. (2022, December). Global perturbation of stratospheric water and aerosol burden by Hunga eruption. *Communications Earth & Environment*, *3*(1), 316. Retrieved from https://doi.org/10.1038/s43247-022-00652-x

Lambert, A., Livesey, N., & Read, W. (2020). *MLS/Aura level 2 nitrous oxide (N2O) mixing ratio V005, Greenbelt, MD, USA, Goddard Earth Sciences Data and Information Services Center (GES DISC), accessed: [26 June 2022]* [dataset]. doi: https://doi.org/10.5067/Aura/MLS/DATA2515

Lambert, A., Livesey, N., Read, W., & Fuller, R. (2021a). *MLS/Aura level 3 daily binned nitrous oxide (N2O) mixing ratio on zonal and similar grids V005, Greenbelt, MD, USA, Goddard Earth Sciences Data and Information Services Center (GES DISC), accessed: [26 June 2022]* [dataset]. Retrieved from https://disc.gsfc.nasa.gov/datasets/ML3DZN2O_005/summary?keywords=mls doi: https://doi.org/10.5067/Aura/MLS/DATA/3116

Lambert, A., Livesey, N., Read, W., & Fuller, R. (2021b). *MLS/Aura level 3 daily binned water vapor (H2O) mixing ratio on zonal and similar grids V005, Greenbelt, MD, USA, Goddard Earth Sciences Data and Information Services Center (GES DISC), accessed: [26 June 2022]* [dataset]. Retrieved from https://disc.gsfc.nasa.gov/datasets/ML3DZH2O_005/summary?keywords=mls doi: https://doi.org/10.5067/Aura/MLS/DATA/3109

Lambert, A., Read, W., & Livesey, N. (2020). *MLS/Aura Level 2 water vapor (H2O) mixing ratio V005, Greenbelt, MD, USA, Goddard Earth Sciences Data and Information Services Center (GES DISC), accessed: [26 June 2022]* [dataset]. doi: https://doi.org/10.5067/Aura/MLS/DATA2508

Lee, J. N., Wu, D. L., Manney, G. L., Schwartz, M. J., Lambert, A., Livesey, N. J., … Read, W. G. (2011). Aura Microwave Limb Sounder observations of the polar middle atmosphere: Dynamics and transport of CO and H_2O. *J. Geophys. Res.*, *116*. doi: 10.1029/2010JD014608

Legras, B., Duchamp, C., Sellitto, P., Podglajen, A., Carboni, E., Siddans, R., … Ploeger, F. (2022, November). The evolution and dynamics of the Hunga Tonga–Hunga Ha'apai sulfate aerosol plume in the stratosphere. *Atmospheric Chemistry and Physics*, *22*(22), 14957–14970. Retrieved 2022-11-23, from https://acp.copernicus.org/articles/22/14957/2022/ (Publisher: Copernicus GmbH) doi: 10.5194/acp-22-14957-2022

Livesey, N. J., Read, W. G., Wagner, P. A., Froidevaux, L., Lambert, A., Manney, G. L., … Lay, R. R. (2020). *EOS MLS version 5.0x level 2 and 3 data quality and description document* (Tech. Rep.). JPL. (Available from http://mls.jpl.nasa.gov/)

Millán, L., et al. (2022). The Hunga Tonga-Hunga Ha'apai hydration of the stratosphere. *Geophys. Res. Lett.*, *49*(13), e2022GL099381. Retrieved from https://agupubs.onlinelibrary.wiley.com/doi/abs/10.1029/2022GL099381 (e2022GL099381 2022GL099381) doi: https://doi.org/10.1029/2022GL099381

Randel, W. J., Moyer, E., Park, M., Jensen, E., Bernath, P., Walker, K., & Boone, C. (2012). Global variations of HDO and HDO/H2O ratios in the upper troposphere and lower stratosphere derived from ACE-FTS satellite measurements. *Journal of Geophysical Research: Atmospheres*, *117*(D6). Retrieved from https://agupubs.onlinelibrary.wiley.com/doi/abs/10.1029/2011JD016632 doi: https://doi.org/10.1029/2011JD016632

Ray, E. A., Moore, F. L., Elkins, J. W., Hurst, D. F., Romashkin, P. A., Dutton, G. S., & Fahey, D. W. (2002). Descent and mixing in the 1999-2000 northern polar vortex inferred from in situ tracer measurments. *J. Geophys. Res.*, *107*, 8285. doi: 10.1029/2001JD000961

Santee, M. L., Lambert, A., Manney, G. L., Livesey, N. J., Froidevaux, L., Neu, J. L., ... Ward, B. M. (2022). Prolonged and pervasive perturbations in the composition of the Southern Hemisphere midlatitude lower stratosphere from the Australian New Year's fires. *Geophysical Research Letters*, *49*(4), e2021GL096270. Retrieved from https://agupubs.onlinelibrary.wiley.com/doi/abs/10.1029/2021GL096270 (e2021GL096270 2021GL096270) doi: https://doi.org/10.1029/2021GL096270

Santee, M. L., MacKenzie, I. A., Manney, G. L., Chipperfield, M. P., Bernath, P. F., Walker, K. A., ... Waters, J. W. (2008). A study of stratospheric chlorine partitioning based on new satellite measurements and modeling. *J. Geophys. Res.*, *113*. doi: 10.1029/2007JD009057

Schoeberl, M. R., Wang, Y., Ueyama, R., Taha, G., Jensen, E., & Yu, W. (2022). Analysis and impact of the Hunga Tonga-Hunga Ha'apai stratospheric water vapor plume. *Geophys. Res. Lett.*, *49*(20), e2022GL100248. Retrieved from https://agupubs.onlinelibrary.wiley.com/doi/abs/10.1029/2022GL100248 (e2022GL100248 2022GL100248) doi: https://doi.org/10.1029/2022GL100248

Schoeberl, M. R., Wang, Y., Ueyama, R., Taha, G., & Yu, W. (2023). The cross equatorial transport of the Hunga Tonga-Hunga Ha'apai eruption plume. *Geophysical Research Letters*, *50*(4), e2022GL102443. Retrieved from https://agupubs.onlinelibrary.wiley.com/doi/abs/10.1029/2022GL102443 (e2022GL102443 2022GL102443) doi: https://doi.org/10.1029/2022GL102443

Schwartz, M., Froidevaux, L., Livesey, N., & Read, W. (2020). *MLS/Aura level 2 ozone (O3) mixing ratio V005, Greenbelt, MD, USA, Goddard Earth Sciences Data and Information Services Center (GES DISC), accessed: [26 june 2022]* [dataset]. doi: https://doi.org/10.5067/Aura/MLS/DATA2506

Schwartz, M., Froidevaux, L., Livesey, N., Read, W., & Fuller, R. (2021). *MLS/Aura level 3 daily binned ozone (O3) mixing ratio on zonal and similar grids V005, Greenbelt, MD, USA, Goddard Earth Sciences Data and Information Services Center (GES DISC), accessed: [26 June 2022]* [dataset]. Retrieved from https://disc.gsfc.nasa.gov/datasets/ML3DZO3_005/summary?keywords=mls doi: https://doi.org/10.5067/Aura/MLS/DATA/3105

Schwartz, M., Pumphrey, H., Livesey, N., & Read, W. (2020). *MLS/Aura level 2 carbon monoxide (CO) mixing ratio V005, Greenbelt, MD, USA, Goddard Earth Sciences Data and Information Services Center (GES DISC), accessed: [26 June 2022]* [dataset]. doi: https://doi.org/10.5067/Aura/MLS/DATA2506

Schwartz, M., Pumphrey, H., Livesey, N., Read, W., & Fuller, R. (2021). *MLS/Aura level 3 daily binned carbon monoxide (CO) mixing ratio on zonal and similar grids V005, Greenbelt, MD, USA, Goddard Earth Sciences Data and Information Services Center (GES DISC), accessed: [26 June 2022]* [dataset]. Retrieved from https://disc.gsfc.nasa.gov/datasets/ML3DZCO_005/summary?keywords=mls doi: https://doi.org/10.5067/Aura/MLS/DATA/3105

Sellitto, P., Podglajen, A., Belhadji, R., Boichu, M., Carboni, E., Cuesta, J., ... Legras, B. (2022, November). The unexpected radiative impact of the Hunga Tonga eruption of 15th January 2022. *Communications Earth & Environment*, *3*(1), 1–10. Retrieved 2022-11-27, from https://www.nature.com/articles/s43247-022-00618-z (Number: 1 Publisher: Nature Publishing Group) doi: 10.1038/s43247-022-00618-z

Sheese, P. E., Walker, K. A., Boone, C. D., Bourassa, A. E., Degenstein, D. A., Froidevaux, L., … Zou, J. (2022). Assessment of the quality of ACE-FTS stratospheric ozone data. *Atmospheric Measurement Techniques*, *15*(5), 1233–1249. Retrieved from https://amt.copernicus.org/articles/15/1233/2022/ doi: 10.5194/amt-15-1233-2022

Taha, G., Loughman, R., Colarco, P. R., Zhu, T., Thomason, L. W., & Jaross, G. (2022). Tracking the 2022 Hunga Tonga-Hunga Ha'apai Aerosol Cloud in the Upper and Middle Stratosphere Using Space-Based Observations. *Geophysical Research Letters*, *49*(19), e2022GL100091. Retrieved 2022-10-13, from https://onlinelibrary.wiley.com/doi/abs/10.1029/2022GL100091 (_eprint: https://onlinelibrary.wiley.com/doi/pdf/10.1029/2022GL100091) doi: 10.1029/2022GL100091

Vömel, H., Evan, S., & Tully, M. (2022, September). Water vapor injection into the stratosphere by Hunga Tonga-Hunga Ha'apai. *Science*, *377*(6613), 1444–1447. Retrieved 2022-11-27, from https://www.science.org/doi/10.1126/science.abq2299 (Publisher: American Association for the Advancement of Science) doi: 10.1126/science.abq2299

Wargan, K., Weir, B., Manney, G. L., Cohn, S. E., & Livesey, N. J. (2020). The anomalous 2019 Antarctic ozone hole in the GEOS constituent data assimilation system with MLS observations. *Journal of Geophysical Research: Atmospheres*, *125*(18), e2020JD033335. Retrieved from https://agupubs.onlinelibrary.wiley.com/doi/abs/10.1029/2020JD033335 (e2020JD033335 2020JD033335) doi: https://doi.org/10.1029/2020JD033335

WMO. (2023). *Scientific assessment of ozone depletion: 2022*. Geneva, Switzerland: Global Ozone Res. and Monit. Proj. Rep. 55.

Zhu, Y., Bardeen, C. G., Tilmes, S., Mills, M. J., Wang, X., Harvey, V. L., … Toon, O. B. (2022, October). Perturbations in stratospheric aerosol evolution due to the water-rich plume of the 2022 Hunga-Tonga eruption. *Communications Earth & Environment*, *3*(1), 1–7. Retrieved 2022-11-27, from https://www.nature.com/articles/s43247-022-00580-w (Number: 1 Publisher: Nature Publishing Group) doi: 10.1038/s43247-022-00580-w

Siege of the South: Hunga Tonga-Hunga Ha'apai Water Vapor Excluded from 2022 Antarctic Stratospheric Polar Vortex

Gloria L. Manney[1,2], Michelle L. Santee[3], Alyn Lambert[3], Luis F. Millán[3], Ken Minschwaner[2], Frank Werner[3], Zachary D. Lawrence[4,5], William G. Read[3], Nathaniel J. Livesey[3], Tao Wang[3]

[1]NorthWest Research Associates, Socorro, NM, USA
[2]New Mexico Institute of Mining and Technology, Socorro, NM, USA
[3]Jet Propulsion Laboratory, California Institute of Technology, Pasadena, CA, USA
[4]Cooperative Institute for Research in Environmental Sciences (CIRES) & NOAA Physical Sciences Laboratory (PSL), University of Colorado, Boulder, Colorado, USA.
[5]NorthWest Research Associates, Boulder, CO, USA

Key Points:

- MLS trace gas data show that the Hunga Tonga-Hunga Ha'apai H_2O plume was effectively excluded from the 2022 Antarctic polar vortex
- Antarctic lower stratospheric vortex strength, size, and longevity were among the largest on record, but within the range of previous years
- Antarctic chemical ozone loss in 2022 was unexceptional, with MLS ozone and related trace gases observed to be near average

Corresponding author: Gloria L Manney, manney@nwra.com

Abstract

We use Aura Microwave Limb Sounder (MLS) trace gas measurements to investigate whether water vapor (H_2O) injected into the stratosphere by the Hunga Tonga-Hunga Ha'apai (HTHH) eruption affected the 2022 Antarctic stratospheric vortex. Other MLS-measured long-lived species are used to distinguish high HTHH H_2O from that descending in the vortex from the upper-stratospheric H_2O peak. HTHH H_2O reached high southern latitudes in June–July but was effectively excluded from the vortex by the strong transport barrier at its edge. MLS H_2O, nitric acid, chlorine species, and ozone within the 2022 Antarctic polar vortex were near average; the vortex was large, strong, and long-lived, but not exceptionally so. There is thus no clear evidence of HTHH influence on the 2022 Antarctic vortex or its composition. Substantial impacts on the stratospheric polar vortices are expected in succeeding years since the H_2O injected by HTHH has spread globally.

Plain Language Summary

The 2022 Hunga Tonga-Hunga Ha'apai eruption injected vast amounts of water vapor into the stratosphere. There has been much speculation that this large increase in water vapor could impact the Antarctic stratospheric polar vortex and Antarctic ozone hole: Water vapor plays an important role in polar vortex ozone depletion by providing the necessary conditions for the formation of polar stratospheric clouds. These clouds provide surfaces on which ozone-depleting chemical reactions can occur. The excess water vapor could also change the vortex evolution via water vapor's effects on temperature, which could in turn affect the strong band of winds demarking the polar vortex edge. We use satellite measurements of water vapor and other gasses to show that by the time the water vapor from the Hunga Tonga volcanic eruption reached the south polar regions in June–July 2022, the polar vortex was too strong for it to penetrate. Measurements of water vapor, ozone, and chemicals involved in destroying ozone all showed near-average amounts and evolution within the vortex. In future years, larger effects on the polar vortex and chemical processing are expected because water vapor from Hunga Tonga that has spread globally will be entrained into the polar vortex.

1 Introduction

The 15 January 2022 eruption of the underwater volcano Hunga Tonga-Hunga Ha'apai (HTHH) injected an unprecedented amount of water vapor (H_2O) directly into the stratosphere, increasing the stratospheric H_2O burden by approximately 10% (e.g., Millán et al., 2022; Vömel et al., 2022). It also resulted in substantial, though not unprecedented, enhancements in volcanic aerosol loading (Khaykin et al., 2022; Sellitto et al., 2022; Taha et al., 2022). Numerous studies have already explored aspects of the stratospheric impacts of HTHH enhancements in aerosol and H_2O; of particular relevance here are suggestions that H_2O and aerosol from HTHH injected into the Southern Hemisphere (SH) stratosphere took many months to reach high latitudes and did not extend poleward of about 60°S (e.g., Legras et al., 2022; Khaykin et al., 2022; Schoeberl et al., 2022; Zhu et al., 2022). In the lowermost stratosphere (at and below approximately the 380 K isentropic surface), a few studies suggest that some H_2O and aerosol were transported to high SH latitudes within days to weeks via the shallow branch of the Brewer-Dobson circulation (e.g. Taha et al., 2022; Schoeberl et al., 2022; Khaykin et al., 2022). Radiative cooling from HTHH H_2O led to unprecedented cold in SH mid/low latitudes, with associated circulation and transport anomalies (Coy et al., 2022; Schoeberl et al., 2022; Sellitto et al., 2022).

It was suggested that transport of HTHH aerosol and H_2O into high SH latitudes might impact the composition of the 2022 SH stratospheric polar vortex, and that circulation changes associated with the HTHH H_2O plume might affect the strength, size, and / or longevity of that vortex (e.g., Taha et al., 2022; Zhu et al., 2022). Here we use Aura Microwave Limb Sounder (MLS) data to analyze the evolution of the SH stratospheric polar vortex in 2022, transport of the HTHH H_2O plume in relation to it, and chemical processing within it. We find no evidence of substantial impacts of HTHH on the 2022 SH polar vortex or the chemical processing and ozone loss within it. We use temperature, H_2O, N_2O, CO, HCl, ClO, and O_3 from v5 MLS "level 3" (L3) data (Livesey et al., 2020), along with meteorological fields from NASA's Modern Era Retrospective-analysis for Research and Applications Version 2 (MERRA-2) dataset (Gelaro et al., 2017; Global Modeling and Assimilation Office (GMAO), 2015).

Immediately following the eruption, standard MLS v5 quality screening (Livesey et al., 2020) flagged many of the profiles most affected by HTHH as suspect retrievals (Millán et al., 2022); thus the H_2O, N_2O, and HNO_3 anomalies shown here may be artificially small for up to three weeks after the eruption. Since our focus is on the subsequent transport and relationship to the SH polar vortex, our results are unaffected.

2 Transport of HTHH Stratospheric H_2O

Figure 1 shows the evolution of N_2O and H_2O (both generally long-lived tracers of transport in the stratosphere) anomalies in the SH lower through middle stratosphere, in vortex averages as a function of height (expressed as potential temperature, θ) and as a function of equivalent latitude (EqL, the latitude enclosing the same area between it and the pole as a given potential vorticity, PV, contour, Butchart & Remsberg, 1986) on several isentropic (θ) surfaces. The past five years include seasons with exceptionally warm / short-lived (2019) and cold / long-lived (2020 and 2021) springtime polar vortices, as well as a year (2018) with more typical vortex characteristics (WMO, 2023). (Figs. S1–S2 in the Supporting Information, SI, show the full-mission and include MLS temperature.) The evolution of vortex-average N_2O (Fig. 1a) in 2022 is unexceptional, showing positive anomalies except at the lowest levels; such a vertical dipole pattern of N_2O anomalies is common, with primarily higher values in 2020, 2021, and 2022 consistent with lower vortex temperatures (see below and Figs. S1–3) and accompanying weaker diabatic descent (Fig. S4). N_2O EqL/time evolution (Fig. 1b–f) is also fairly typical; recurring changes above 430 K from high to low anomalies extending from low latitudes show quasi-biennial oscillation (QBO) related transport (e.g.. Baldwin et al., 2001; Diallo et al., 2019). Low N_2O anomalies in austral spring 2020 and 2021 are related to the delayed vortex breakup in those years, with low N_2O values remaining confined longer in a more persistent vortex. Spring 2022 shows similar, but weaker, anomalies, suggesting a long-lived vortex. In contrast, high anomalies in 2019 result from a rare SH sudden stratospheric warming that led to a small, warm, and short-lived vortex (e.g., Wargan et al., 2020).

H_2O anomalies (Fig. 1g–l) in the SH lower stratospheric vortex are typically dominated by interannual variations in polar stratospheric cloud extent; strong low H_2O anomalies in spring 2020 and 2021 at 500 K and surrounding levels arose from persistent cold anomalies in unusually long-lasting vortices. Outside the vortex (Fig. 1h–lFig. 1g–l), high H_2O anomalies often accompany low N_2O anomalies because H_2O and N_2O have opposite vertical and horizontal gradients in the lower to middle stratosphere. For example, low (high) springtime H_2O (N_2O) anomalies just outside the vortex edge in 2019, and opposite patterns in 2020 and 2021 at 600–850 K; similar patterns are seen in mid-Eqls in earlier years (Fig. S1). (Note that typical H_2O anomalies prior to 2022 are washed out by the large colorbar range needed to portray the HTHH H_2O.) Above 500 K, typical signatures of extra-vortex transport of H_2O are overwhelmed by the arrival of HTHH H_2O (Fig. 1h–j, Fig. S1). HTHH H_2O reached the vortex edge in early June 2022, after the vortex was fully developed except in the lowermost stratosphere. Above 500 K, extremely strong gradients along the vortex edge suggest that the HTHH plume could not penetrate the vortex edge. Pervasive high H_2O anomalies since early 2020 below about 500 K may reflect lingering enhancements from the 2020 Australian New Years fires (e.g., Santee et al., 2022). While small positive anomalies encroach into the vortex region in late winter 2022 at 500 K (near the lowest altitude of large HTHH enhancement) and 430 K, similar features are common (e.g., in 2018 and 2021), so it is unclear whether they are related to the HTHH plume. At all levels examined (including the lowermost stratosphere, e.g., Fig. S3), H_2O anomalies inside the vortex are within the typical range.

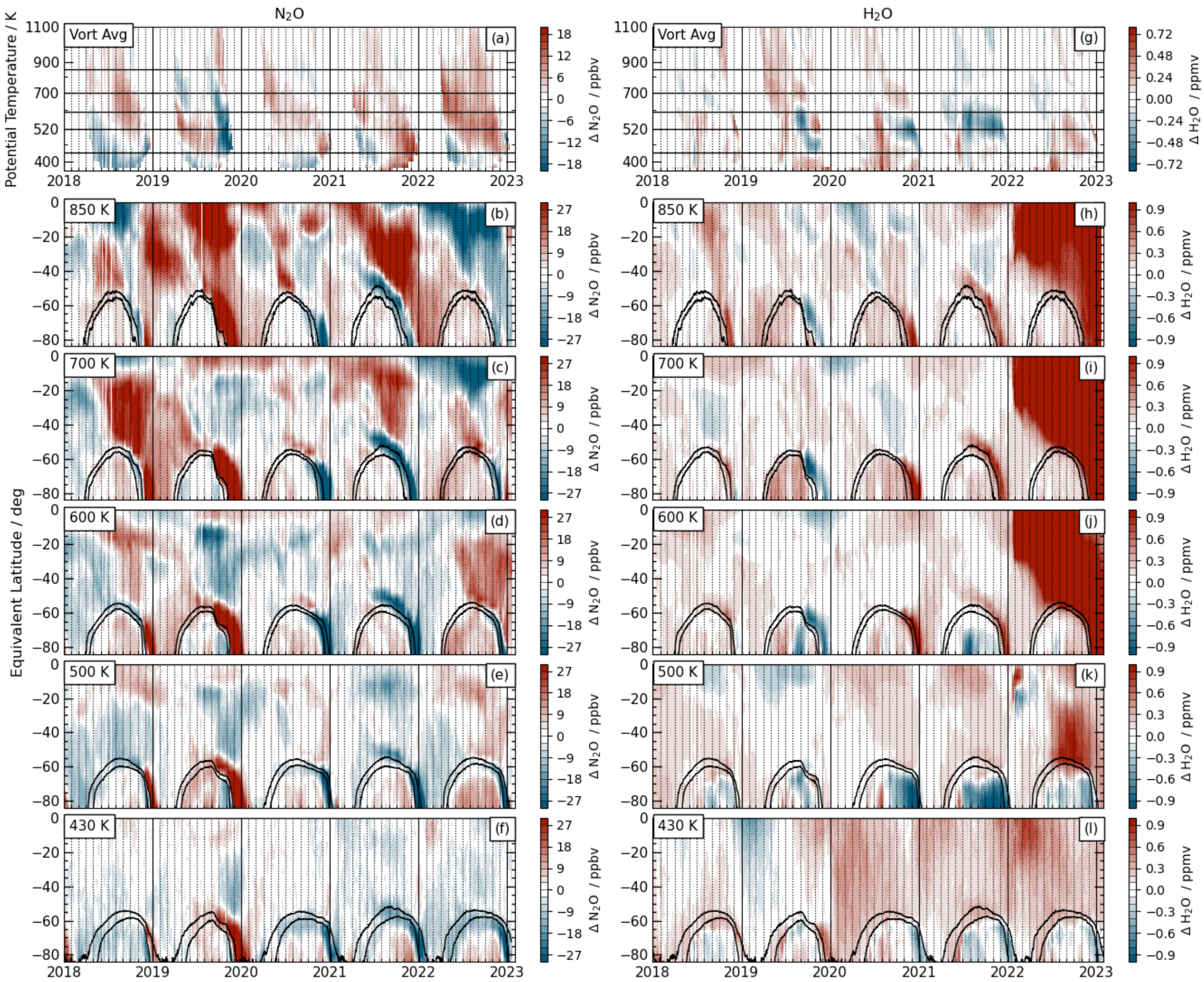

Figure 1. Evolution of MLS-observed SH anomalies from the baseline 2005–2021 climatology of N_2O (a–f) and H_2O (g–l) from January 2018 through January 2023: (a,g) vortex-averaged values; (b–f, h–l) evolution as a function of EqL at levels in the middle through lower stratosphere (horizontal lines in a,g). Black contours in b–f and h–l are sPV values indicating the vortex edge region.

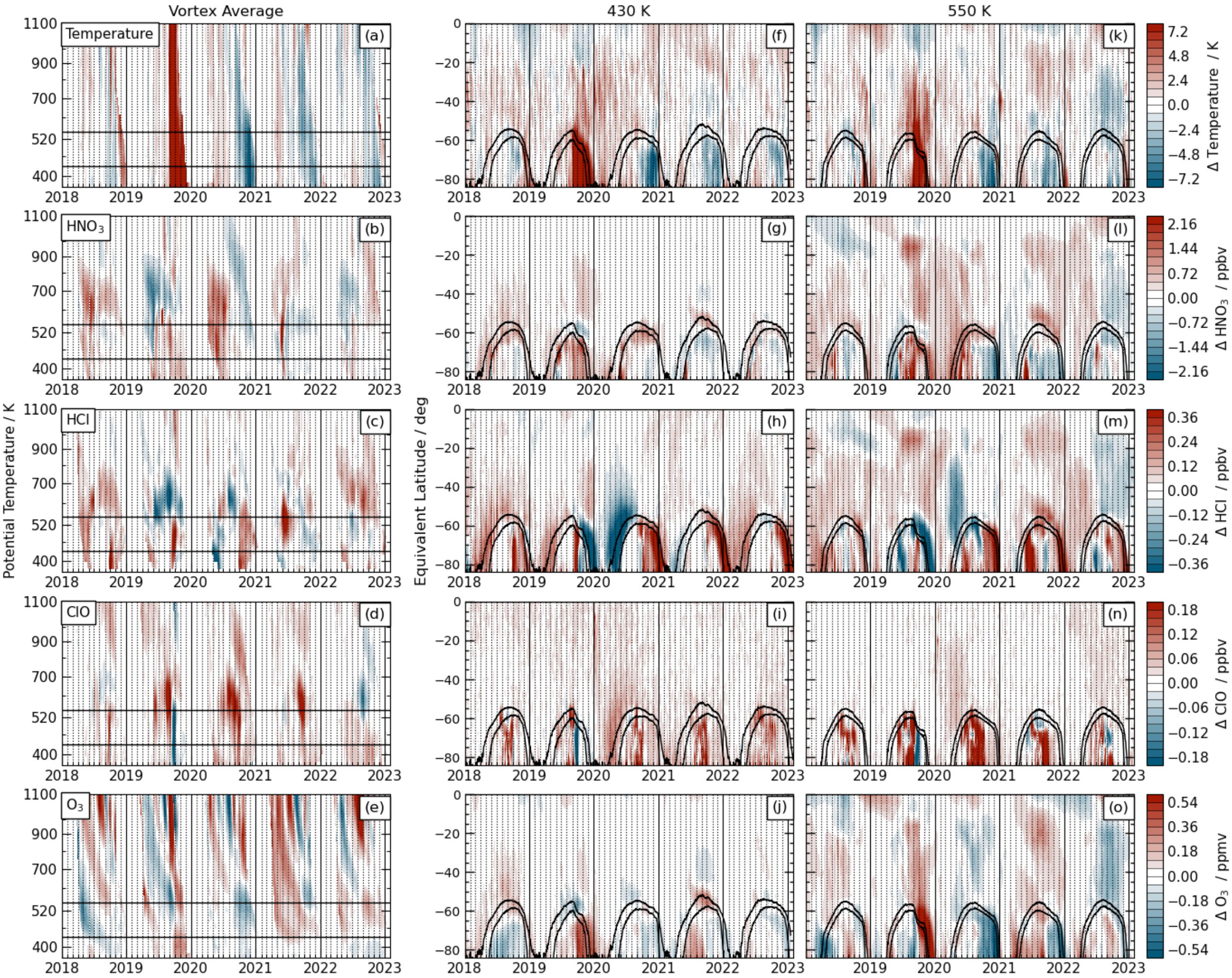

Figure 2. As in Fig. 1, but for MLS temperature, HNO_3, HCl, ClO, and O_3; (a–e) vortex averages, (f–j) 430 K, and (k–o) 550 K EqL timeseries, for January 2018 through January 2023. Black contours (f–o) are sPV values demarking the vortex edge region.

3 Polar Vortex Composition and Chemical Processing

Figure 2 shows a similar view of MLS measurements of temperature and species involved in polar chemical processing (Figs. S1–3 show 550 K, 430 K, and 380 K for the full mission). The Antarctic vortex was unusually cold and persistent in spring 2022, but less so than in 2020 and 2021. Vortex HNO_3 values were near average throughout the season. Vortex HCl and ClO commonly oscillate between high and low anomalies, and thus they are also generally unexceptional within the 2022 vortex; the high HCl anomalies in spring are related primarily to longer-than-usual confinement of the very high values that ensue from chlorine deactivation. Consistent with near-average vortex values of chlorine species, O_3 anomalies in 2022 were also relatively small. Both 2020 and 2021 showed lower O_3, consistent with larger cold anomalies and even longer-lived (see below) vortices in those years than in 2022. Outside the vortex, temperature anomalies (arising from radiative effects of HTHH H_2O, e.g., Coy et al., 2022; Schoeberl et al., 2022) and associated mid-latitude transport anomalies (Coy et al., 2022) appear consistent with the extravortex high N_2O anomalies seen near 500–600 K (Fig. 1), and suggest that accompanying extravortex HCl, HNO_3, and O_3 anomalies are at least partially transport-driven.

Figure 3 provides a closer look at the EqL/θ evolution of MLS trace gases in 2022, showing snapshots of anomalies from climatology (similar anomaly plots in 2018, 2020, and 2021 are shown in Figs. S5–S7). The H_2O plume first approached the SH polar vortex edge in early to mid-June. Subsequently, extremely strong H_2O gradients developed along the vortex edge over 520–800 K and persisted through October (into December below about 700 K; see also Fig 1). By mid-December, only a weak remnant of the vortex remained below about 520 K, and the H_2O enhancement extended into high latitudes above that level. MLS data show no indication of air from the HTHH H_2O plume penetrating substantially into the SH vortex before its breakup. N_2O anomalies within the vortex were generally small until austral spring; below about 700 K, these anomalies were near zero from August through October. Low N_2O anomalies along the vortex edge beginning in early November are consistent with confinement in an unusually persistent vortex. Mid-latitude cold anomalies throughout the middle stratosphere (e.g., Coy et al., 2022; Schoeberl et al., 2022) are apparent from June through mid-December. Vortex temperatures were below average through much of the season, with largest cold anomalies in October and November (also see Fig. 2). High extra-vortex N_2O anomalies through this period are consistent in extent and location with the circulation anomalies reported by Coy et al. (2022). The co-location of N_2O anomalies with those in HNO_3, HCl, and O_3 suggests that transport plays a role in all of them; work is in progress analyzing the relative effects of dynamical and chemical processes.

Within the vortex, HNO_3 is slightly lower than usual, consistent with a colder-than-average vortex. HCl (ClO) shows low (high) anomalies during much (but not all, e.g., Fig. 3A,G) of the winter. As noted above, high HCl anomalies appear along the vortex edge in November and in the vortex remnant in mid-December, consistent with high values resulting from deactivation into HCl (as is typical in the SH, e.g., Santee et al., 2008) followed by unusually enduring confinement in the persistent vortex. Lower stratospheric O_3 anomalies in the early winter (before extensive chemical loss) are slightly positive and remain so through October (e.g., Fig. 3O). Taken together, the results in Figs. 2 and 3 suggest that the modest low anomalies in O_3 seen in austral spring 2022 (e.g., Fig. 3P) result primarily (if not entirely) from the unusual persistence of the vortex.

4 Vortex Evolution and Trace Gas Confinement

Figure 4 summarizes the evolution of the 2022 SH vortex in the context of the 43-year MERRA-2 record and the evolution of trace gases in the context of the 18-year MLS record, both in relation to the previous three SH winters. Figure S8 shows profiles of additional MERRA-2 diagnostics of vortex strength and longevity. Consistent with the indications in the trace gases of its unusual persistence, the 2022 SH late winter and spring vortex was among the largest on record at levels up to about 650 K, approximately matching the maximum size and persistence seen prior to 2020 (Fig. 4a–d; Fig. S8b,d). In spring, the 2021 vortex area was slightly larger, and the 2020 vortex area substantially larger than that in 2022 from about 460 K to 650 K, with 2020 setting the record for lower-stratospheric vortex persistence (Fig. 4a–c, S8b–d). Maximum PV gradients, indicating vortex strength (that is, robustness as a transport barrier), show unusually strong springtime vortices in 2020 through 2022 below about 500 K, but only the 2020 vortex was stronger than average above about 600 K (Fig. 4e–h; Fig. S8a). Below about 520 K, the area with temperatures below the nitric acid trihydrate (NAT) and ice polar stratospheric cloud (PSC) thresholds was larger than usual (Fig 4m,n,q,r) and PSCs persisted later than usual (Fig. 4m–t, Fig. S8e,f) in spring 2020, 2021, and 2022, but only exceeded previous springtime records in 2020; above about 600 K PSC area and duration were near average.

The unexceptional MLS trace gas evolution in the 2022 Antarctic vortex is highlighted in Fig. 4A–P (Fig. S9 shows the vertical structure). Interannual variability in SH polar chemical processing is relatively small, but, with few exceptions, all of the trace gases show 2022 evolution that is well within the previously observed range. Over $\sim$450–600 K, persistently low H_2O after October in 2022, and to an even greater extent in 2020 and 2021, is consistent with confinement of dehydrated air in long-lived vortices. Chlorine evolution (seen in HCl and ClO, Fig. 4E–

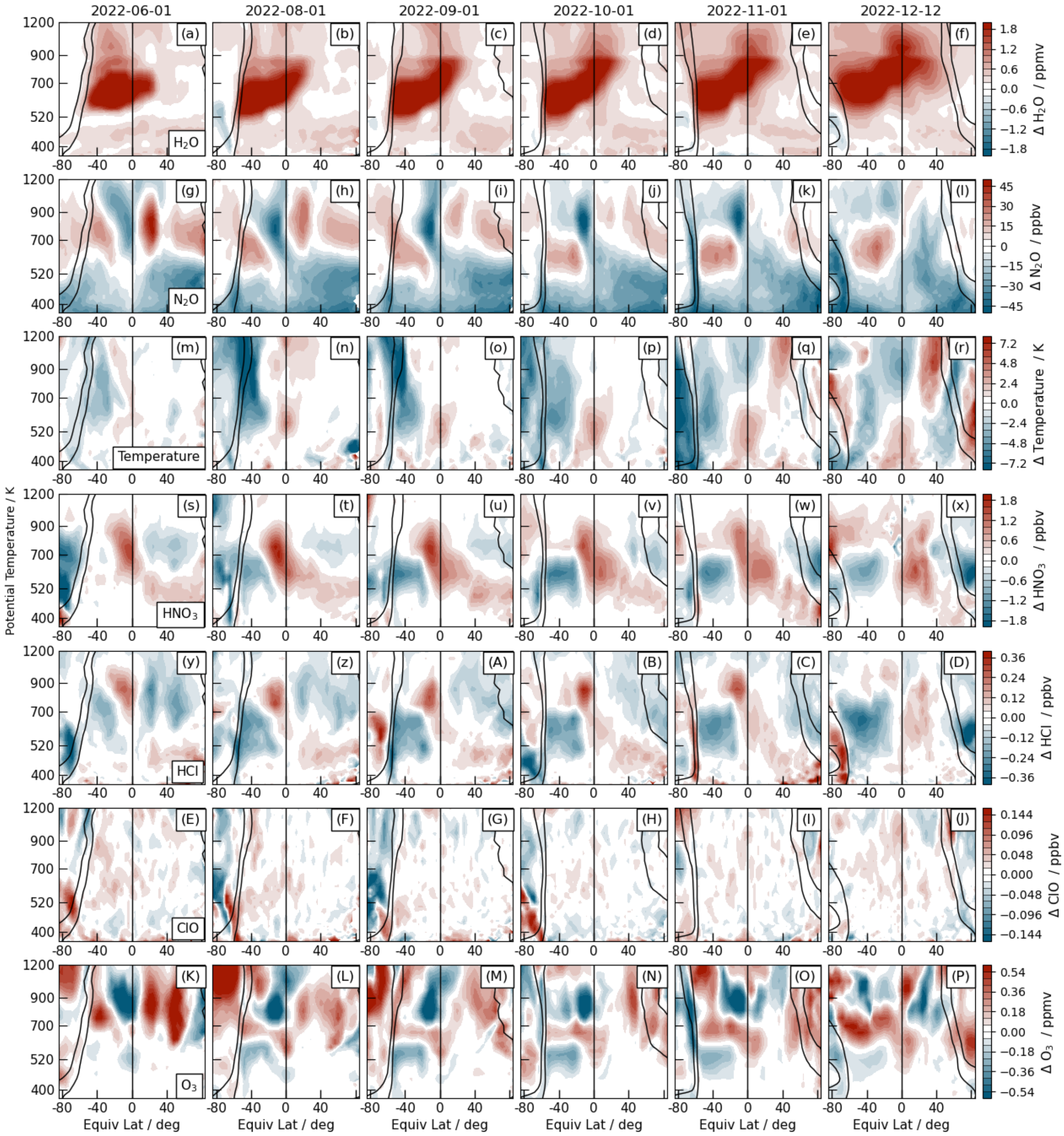

Figure 3. Snapshots on selected days in 2022 of anomalies from the baseline 2005–2021 climatology of MLS (a–f) H_2O, (g–l) N_2O, (m–r) temperature, (s–x) HNO_3, (y–D) HCl, (E–J) ClO, and (K–P) O_3. Black contours show sPV values demarking the vortex edge region.

L; Fig. S9q–x) was fairly typical throughout the season. Observed O_3 evolution in 2022 was remarkably near average throughout the season (Fig. 4M–P; Fig. S9y–B).

The above results provide visual evidence that the vortex edge presented an effective transport barrier, preventing substantial penetration of the HTHH H_2O plume. To look more closely at the robustness of the vortex edge transport barrier, Fig. 5 shows scatter and density plots of H_2O versus N_2O and sPV for representative days in 2022 compared with the evolution in all prior years in the MLS record. Low N_2O (relative to the range of values at a given level) and high-magnitude sPV identify vortex air parcels. In the lower stratosphere (exemplified by 550 K), increasingly low vortex H_2O through the season results from dehydration and is very similar to that previously observed by MLS (density plots, right columns, emphasize the similarity of the main distributions in 2022 to those in earlier years). Extravortex H_2O at 550 K does not stand out from the previous record before July, but after that the HTHH enhancement manifests as a distinct cluster of high H_2O with N_2O near 200 ppbv and sPV magnitudes $<1\times10^{-4}$ s^{-1} (both values that are unambiguously extravortex) that is unique to 2022 (compare yellow-orange / purple H_2O / sPV values with grey dots; orange with grey contours). In the middle stratosphere (exemplified by 700 K), vortex H_2O values first increase via descent of the upper stratospheric peak, then decrease as continuing descent brings low mesospheric H_2O into the stratospheric vortex (e.g., Ray et al., 2002; Lee et al., 2011); both the high (e.g., Fig. 5a–d) and the low (e.g., Fig. 5e–l) H_2O values that descend through the vortex (low N_2O, high-magnitude sPV end of the x-axis) at 700 K are distinct from the extravortex population of high H_2O from HTHH, and that is in turn distinguished from extravortex air in previous years by higher H_2O values at extravortex N_2O ($\sim$150–200 ppbv) and sPV (magnitude $<\sim1\times10^{-4}$ s^{-1}). These correlations of H_2O with N_2O and sPV (especially the density plots versus sPV) show clearly that the air with enhanced H_2O from HTHH remained well separated from that within the vortex until vortex breakup at each level (as suggested in Figs. 1 and 3). MLS H_2O / CO correlations show a similar picture in the middle (Fig. S10) and upper stratosphere, with HTHH H_2O associated with low CO values characteristic of extravortex air. Further, because the seawater from HTHH has a higher ratio of HDO to H_2O than background water vapor in the extravortex stratosphere (e.g., Randel et al., 2012; Khaykin et al., 2022), an unprecedented increase in that ratio in SH midlatitudes also marks the HTHH air as separate from (and excluded from) that in the vortex (Figs. S11–12).

5 Summary

The unprecedented water vapor injection into the stratosphere by HTHH is tracked using MLS and reanalysis data. The H_2O plume [[or The enhanced H_2O]] is shown to have been effectively excluded from the 2022 Antarctic polar vortex until the vortex breakdown. In contrast to speculation that HTHH stratospheric H_2O and aerosol injections would lead to substantial anomalies in the Antarctic polar vortex and lower stratospheric polar processing and ozone loss within it (e.g., Taha et al., 2022; Zhu et al., 2022), our analysis suggests that HTHH did not cause substantial changes in polar processing and ozone loss within the vortex: MLS observations of HNO_3, HCl, ClO, and O_3 inside the vortex through the depth of the lower stratosphere all show evolution well within the range of previous years during the MLS mission, with near-average O_3 loss. Evidence for possible dynamical impacts on the vortex is likewise not unequivocal: The vortex was among the larger, stronger, and longer-lived in the SH lower stratosphere, but these conditions were matched or exceeded by those in 2020, 2021, and several previous years in the MERRA-2 record since 1980; vortex cold anomalies were even less exceptional. Thus, despite large radiative, dynamical, and composition perturbations in midlatitudes, the observational evidence shows that chemical processing within the 2022 Antarctic stratospheric polar vortex was fairly typical, and does not show clear evidence of substantial dynamical vortex perturbations. The dispersal of HTHH H_2O following the Antarctic vortex breakup (e.g., Fig. 1) led to unprecedented high H_2O anomalies throughout the SH, which are expected to linger for at least several years (e.g., Millán et al., 2022; Khaykin et al., 2022), raising the expectation of large perturbations to Antarctic polar vortex chemistry and the ozone hole in 2023 and beyond. HTHH H_2O has also been transported into the Northern Hemisphere (e.g., Schoeberl et al., 2023), but reached the Arctic vor-

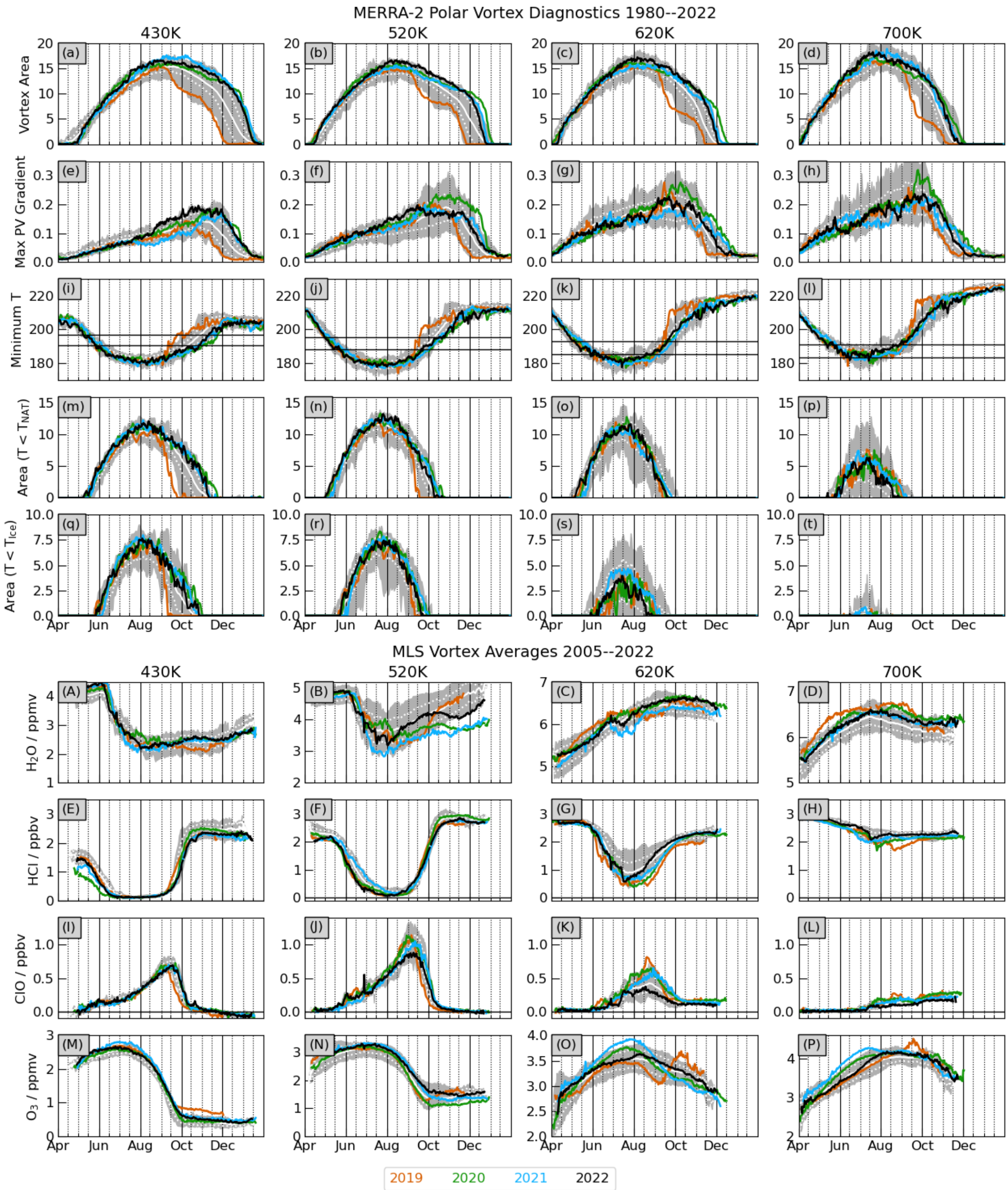

Figure 4. (a–t) Time series at four levels in the lower to middle stratosphere of vortex area, maximum PV gradients, high latitude (poleward of 30°) minimum temperature, and area below NAT and ice PSC thresholds, comparing 2019 (orange), 2020 (green), 2021 (cyan), and 2022 (black) with the range (shading), mean (solid white line), and one standard deviation envelope (dotted white lines) over 1980–2018. (A–P) Vortex-averaged H_2O, HCl, ClO, and O_3 in same format as for the dynamical fields, with the range over 2005–2018.

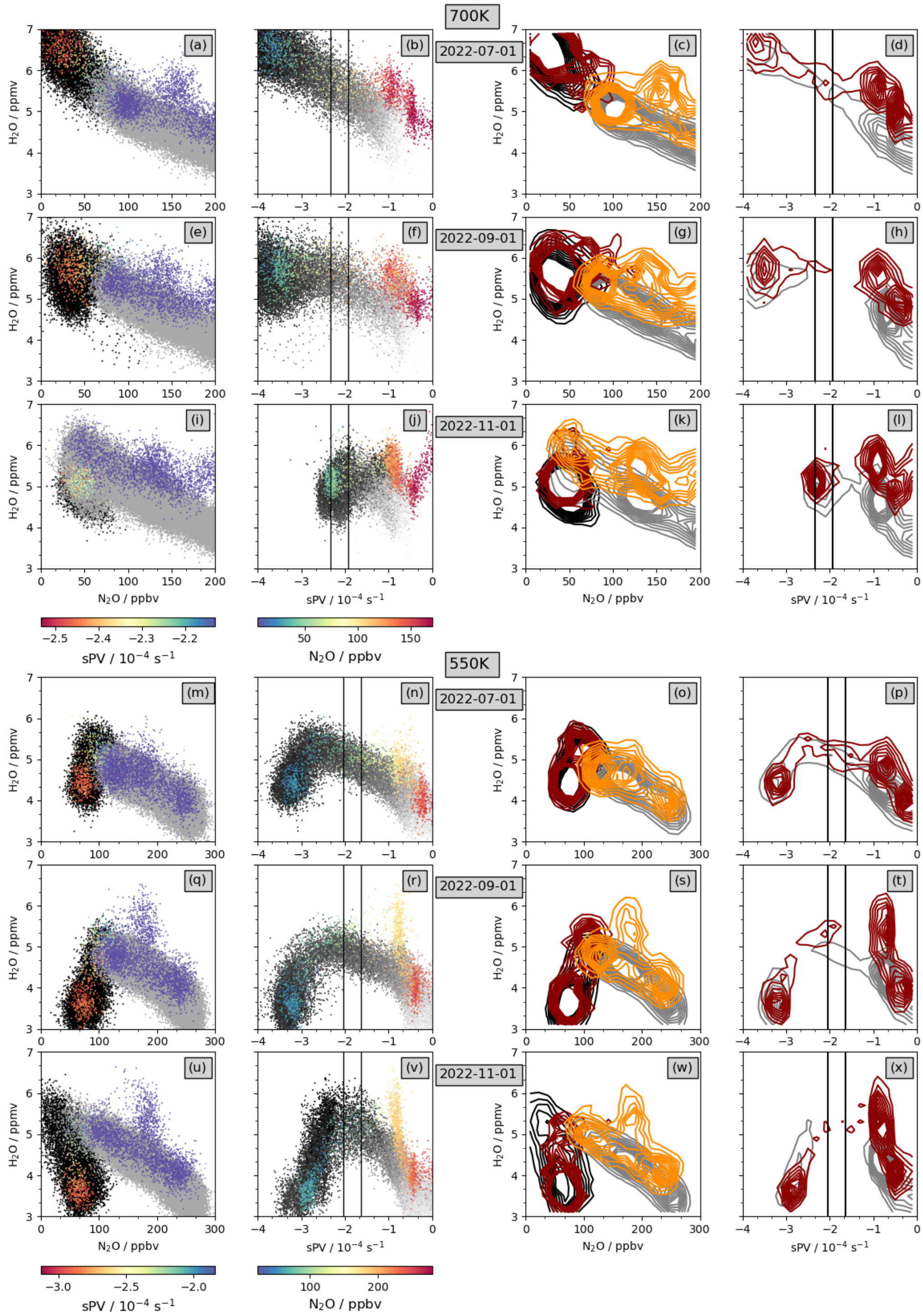

Figure 5. Scatter (left two columns) and density (right two columns) plots of MLS H_2O (y-axis) versus N_2O (first and third columns) and sPV (second and last columns). Grey and black dots (contours) show values from 2005–2021 in the scatter (density) plots; for those years, black (grey) indicates x-axis values of N_2O or sPV characteristic of inside (outside) the vortex. For 2022, colored (purple) dots or dark red (orange) contours show sPV values inside (outside) the vortex. 2022 N_2O (second column) is colored such that blue/blue-green shows typical vortex values. Black vertical lines on the plots versus sPV indicate the vortex edge region.

tex edge after the vortex was well-developed and was only dispersed through the NH after a strong sudden stratospheric warming starting in mid-February (paper in preparation). Thus large effects on Arctic polar vortex chemistry are also expected to manifest starting in the 2023/2024 cool season.

6 Open Research

The data used herein are publicly available as follows:

- MERRA-2: (Global Modeling and Assimilation Office (GMAO), 2015) `https://disc.sci.gsfc.nasa.gov/uui/datasets?keywords=%22MERRA-2%22`
- Aura MLS Level-2 and Level-3 data: (Lambert, Read, & Livesey, 2020; Lambert, Livesey, & Read, 2020; Lambert et al., 2021b, 2021a; Schwartz, Pumphrey, et al., 2020; Schwartz, Froidevaux, et al., 2020; Schwartz, Pumphrey, et al., 2021; Schwartz, Froidevaux, et al., 2021) `https://disc.gsfc.nasa.gov/datasets?page=1&keywords=AURA%20MLS`
- ACE-FTS v4.1/4.2 data: `http://www.ace.uwaterloo.ca` (registration required)
- ACE-FTS v4.1/4.2 error flags: `https://dataverse.scholarsportal.info/api/access/dataset/:persistentId/versions/:latest?persistentId=doi:10.5683/SP2/BC4ATC`
- MLS & ACE-FTS derived meteorological products: `https://mls.jpl.nasa.gov/eos-aura-mls/dmp` (registration required).

Acknowledgments

Thanks to the MLS team at JPL for data processing and analysis support, especially Brian Knosp for data management, Ryan Fuller for development and production of the MLS L3 products, and Lucien Froidevaux and Michael Schwartz for helpful discussions. Thanks to the ACE science team for making the ACE-FTS data available, especially Kaley Walker and Patrick Sheese for advice on data quality and usage. Thanks to the GMAO for providing the MERRA-2 dataset. G.L. Manney was supported by the Jet Propulsion Laboratory (JPL) Microwave Limb Sounder team under JPL subcontract #1521127 to NWRA. Work at the Jet Propulsion Laboratory, California Institute of Technology, was carried out under a contract with the National Aeronautics and Space Administration (80NM0018D0004).

References

Baldwin, M. P., Gray, L. J., Dunkerton, T. J., Hamilton, K., Haynes, P. H., J, W., … Takahasi, M. (2001). The quasi-biennial oscillation. *Rev. Geophys.*, *39*, 179–229.

Boone, C., Bernath, P., Cok, D., Jones, S., & Steffen, J. (2020). Version 4 retrievals for the atmospheric chemistry experiment Fourier transform spectrometer (ACE-FTS) and imagers. *Journal of Quantitative Spectroscopy and Radiative Transfer*, *247*, 106939. Retrieved from `https://www.sciencedirect.com/science/article/pii/S0022407319305916` doi: https://doi.org/10.1016/j.jqsrt.2020.106939

Butchart, N., & Remsberg, E. E. (1986). The area of the stratospheric polar vortex as a diagnostic for tracer transport on an isentropic surface. *J. Atmos. Sci.*, *43*, 1319–1339.

Coy, L., Newman, P. A., Wargan, K., Partyka, G., Strahan, S. E., & Pawson, S. (2022). Stratospheric Circulation Changes Associated With the Hunga Tonga-Hunga Ha'apai Eruption. *Geophysical Research Letters*, *49*(22), e2022GL100982. Retrieved 2022-11-27, from `https://onlinelibrary.wiley.com/doi/abs/10.1029/2022GL100982` (_eprint: https://onlinelibrary.wiley.com/doi/pdf/10.1029/2022GL100982) doi: 10.1029/2022GL100982

Diallo, M., Konopka, P., Santee, M. L., Müller, R., Tao, M., Walker, K. A., … Ploeger,

F. (2019). Structural changes in the shallow and transition branch of the Brewer–Dobson circulation induced by El Niño. *Atmos. Chem. Phys.*, *19*(1), 425–446. Retrieved from https://acp.copernicus.org/articles/19/425/2019/ doi: 10.5194/acp-19-425-2019

Gelaro, R., McCarty, W., Suárez, M. J., Todling, R., Molod, A., Takacs, L., … Zhao, B. (2017). The Modern-Era Retrospective Analysis for Research and Applications, Version-2 (MERRA-2). *J. Clim.*, *30*, 5419–5454. doi: doi:10.1175/JCLI-D-16-0758.1

Global Modeling and Assimilation Office (GMAO). (2015). *MERRA-2 inst3_3d_asm_nv: 3d, 3-hourly,instantaneous, model-level, assimilation, assimilated meteorological fields v5.12.4, Greenbelt, MD, USA, Goddard Earth Sciences Data and Information Services Center (GES DISC), accessed 1 June 2022* [dataset]. doi: 10.5067/WWQSXQ8IVFW8

Khaykin, S., Podglajen, A., Ploeger, F., Grooß, J.-U., Tence, F., Bekki, S., … Ravetta, F. (2022, December). Global perturbation of stratospheric water and aerosol burden by Hunga eruption. *Communications Earth & Environment*, *3*(1), 316. Retrieved from https://doi.org/10.1038/s43247-022-00652-x

Lambert, A., Livesey, N., & Read, W. (2020). *MLS/Aura level 2 nitrous oxide (N2O) mixing ratio V005, Greenbelt, MD, USA, Goddard Earth Sciences Data and Information Services Center (GES DISC), accessed: [26 June 2022]* [dataset]. doi: https://doi.org/10.5067/Aura/MLS/DATA2515

Lambert, A., Livesey, N., Read, W., & Fuller, R. (2021a). *MLS/Aura level 3 daily binned nitrous oxide (N2O) mixing ratio on zonal and similar grids V005, Greenbelt, MD, USA, Goddard Earth Sciences Data and Information Services Center (GES DISC), accessed: [26 June 2022]* [dataset]. Retrieved from https://disc.gsfc.nasa.gov/datasets/ML3DZN2O_005/summary?keywords=mls doi: https://doi.org/10.5067/Aura/MLS/DATA/3116

Lambert, A., Livesey, N., Read, W., & Fuller, R. (2021b). *MLS/Aura level 3 daily binned water vapor (H2O) mixing ratio on zonal and similar grids V005, Greenbelt, MD, USA, Goddard Earth Sciences Data and Information Services Center (GES DISC), accessed: [26 June 2022]* [dataset]. Retrieved from https://disc.gsfc.nasa.gov/datasets/ML3DZH2O_005/summary?keywords=mls doi: https://doi.org/10.5067/Aura/MLS/DATA/3109

Lambert, A., Read, W., & Livesey, N. (2020). *MLS/Aura Level 2 water vapor (H2O) mixing ratio V005, Greenbelt, MD, USA, Goddard Earth Sciences Data and Information Services Center (GES DISC), accessed: [26 June 2022]* [dataset]. doi: https://doi.org/10.5067/Aura/MLS/DATA2508

Lee, J. N., Wu, D. L., Manney, G. L., Schwartz, M. J., Lambert, A., Livesey, N. J., … Read, W. G. (2011). Aura Microwave Limb Sounder observations of the polar middle atmosphere: Dynamics and transport of CO and H_2O. *J. Geophys. Res.*, *116*. doi: 10.1029/2010JD014608

Legras, B., Duchamp, C., Sellitto, P., Podglajen, A., Carboni, E., Siddans, R., … Ploeger, F. (2022, November). The evolution and dynamics of the Hunga Tonga–Hunga Ha'apai sulfate aerosol plume in the stratosphere. *Atmospheric Chemistry and Physics*, *22*(22), 14957–14970. Retrieved 2022-11-23, from https://acp.copernicus.org/articles/22/14957/2022/ (Publisher: Copernicus GmbH) doi: 10.5194/acp-22-14957-2022

Livesey, N. J., Read, W. G., Wagner, P. A., Froidevaux, L., Lambert, A., Manney, G. L., … Lay, R. R. (2020). *EOS MLS version 5.0x level 2 and 3 data quality and description document* (Tech. Rep.). JPL. (Available from http://mls.jpl.nasa.gov/)

Millán, L., et al. (2022). The Hunga Tonga-Hunga Ha'apai hydration of the stratosphere. *Geophys. Res. Lett.*, *49*(13), e2022GL099381. Retrieved from https://agupubs.onlinelibrary.wiley.com/doi/abs/10.1029/2022GL099381 (e2022GL099381 2022GL099381) doi: https://doi.org/10.1029/2022GL099381

Randel, W. J., Moyer, E., Park, M., Jensen, E., Bernath, P., Walker, K., & Boone, C. (2012). Global variations of HDO and HDO/H2O ratios in the upper troposphere and lower stratosphere derived from ACE-FTS satellite measurements. *Journal of Geophysical Research: Atmospheres*, *117*(D6). Retrieved from https://agupubs.onlinelibrary.wiley.com/doi/abs/10.1029/2011JD016632 doi: https://doi.org/10.1029/2011JD016632

Ray, E. A., Moore, F. L., Elkins, J. W., Hurst, D. F., Romashkin, P. A., Dutton, G. S., & Fahey, D. W. (2002). Descent and mixing in the 1999-2000 northern polar vortex inferred from in situ tracer measurments. *J. Geophys. Res.*, *107*, 8285. doi: 10.1029/2001JD000961

Santee, M. L., Lambert, A., Manney, G. L., Livesey, N. J., Froidevaux, L., Neu, J. L., … Ward, B. M. (2022). Prolonged and pervasive perturbations in the composition of the Southern Hemisphere midlatitude lower stratosphere from the Australian New Year's fires. *Geophysical Research Letters*, *49*(4), e2021GL096270. Retrieved from https://agupubs.onlinelibrary.wiley.com/doi/abs/10.1029/2021GL096270 (e2021GL096270 2021GL096270) doi: https://doi.org/10.1029/2021GL096270

Santee, M. L., MacKenzie, I. A., Manney, G. L., Chipperfield, M. P., Bernath, P. F., Walker, K. A., … Waters, J. W. (2008). A study of stratospheric chlorine partitioning based on new satellite measurements and modeling. *J. Geophys. Res.*, *113*. doi: 10.1029/2007JD009057

Schoeberl, M. R., Wang, Y., Ueyama, R., Taha, G., Jensen, E., & Yu, W. (2022). Analysis and impact of the Hunga Tonga-Hunga Ha'apai stratospheric water vapor plume. *Geophys. Res. Lett.*, *49*(20), e2022GL100248. Retrieved from https://agupubs.onlinelibrary.wiley.com/doi/abs/10.1029/2022GL100248 (e2022GL100248 2022GL100248) doi: https://doi.org/10.1029/2022GL100248

Schoeberl, M. R., Wang, Y., Ueyama, R., Taha, G., & Yu, W. (2023). The cross equatorial transport of the Hunga Tonga-Hunga Ha'apai eruption plume. *Geophysical Research Letters*, *50*(4), e2022GL102443. Retrieved from https://agupubs.onlinelibrary.wiley.com/doi/abs/10.1029/2022GL102443 (e2022GL102443 2022GL102443) doi: https://doi.org/10.1029/2022GL102443

Schwartz, M., Froidevaux, L., Livesey, N., & Read, W. (2020). *MLS/Aura level 2 ozone (O3) mixing ratio V005, Greenbelt, MD, USA, Goddard Earth Sciences Data and Information Services Center (GES DISC), accessed: [26 june 2022]* [dataset]. doi: https://doi.org/10.5067/Aura/MLS/DATA2506

Schwartz, M., Froidevaux, L., Livesey, N., Read, W., & Fuller, R. (2021). *MLS/Aura level 3 daily binned ozone (O3) mixing ratio on zonal and similar grids V005, Greenbelt, MD, USA, Goddard Earth Sciences Data and Information Services Center (GES DISC), accessed: [26 June 2022]* [dataset]. Retrieved from https://disc.gsfc.nasa.gov/datasets/ML3DZO3_005/summary?keywords=mls doi: https://doi.org/10.5067/Aura/MLS/DATA/3105

Schwartz, M., Pumphrey, H., Livesey, N., & Read, W. (2020). *MLS/Aura level 2 carbon monoxide (CO) mixing ratio V005, Greenbelt, MD, USA, Goddard Earth Sciences Data and Information Services Center (GES DISC), accessed: [26 June 2022]* [dataset]. doi: https://doi.org/10.5067/Aura/MLS/DATA2506

Schwartz, M., Pumphrey, H., Livesey, N., Read, W., & Fuller, R. (2021). *MLS/Aura level 3 daily binned carbon monoxide (CO) mixing ratio on zonal and similar grids V005, Greenbelt, MD, USA, Goddard Earth Sciences Data and Information Services Center (GES DISC), accessed: [26 June 2022]* [dataset]. Retrieved from https://disc.gsfc.nasa.gov/datasets/ML3DZCO_005/summary?keywords=mls doi: https://doi.org/10.5067/Aura/MLS/DATA/3105

Sellitto, P., Podglajen, A., Belhadji, R., Boichu, M., Carboni, E., Cuesta, J., … Legras, B. (2022, November). The unexpected radiative impact of the Hunga Tonga eruption of 15th January 2022. *Communications Earth & Environment*, *3*(1), 1–10. Retrieved 2022-11-27, from https://www.nature.com/articles/s43247-022-00618-z (Number: 1 Publisher: Nature Publishing Group) doi: 10.1038/s43247-022-00618-z

Sheese, P. E., Walker, K. A., Boone, C. D., Bourassa, A. E., Degenstein, D. A., Froidevaux, L., … Zou, J. (2022). Assessment of the quality of ACE-FTS stratospheric ozone data. *Atmospheric Measurement Techniques*, *15*(5), 1233–1249. Retrieved from https://amt.copernicus.org/articles/15/1233/2022/ doi: 10.5194/amt-15-1233-2022

Taha, G., Loughman, R., Colarco, P. R., Zhu, T., Thomason, L. W., & Jaross, G. (2022). Tracking the 2022 Hunga Tonga-Hunga Ha'apai Aerosol Cloud in the Upper and Middle Stratosphere Using Space-Based Observations. *Geophysical Research Letters*, *49*(19), e2022GL100091. Retrieved 2022-10-13, from https://onlinelibrary.wiley.com/doi/abs/10.1029/2022GL100091 (_eprint: https://onlinelibrary.wiley.com/doi/pdf/10.1029/2022GL100091) doi: 10.1029/2022GL100091

Vömel, H., Evan, S., & Tully, M. (2022, September). Water vapor injection into the stratosphere by Hunga Tonga-Hunga Ha'apai. *Science*, *377*(6613), 1444–1447. Retrieved 2022-11-27, from https://www.science.org/doi/10.1126/science.abq2299 (Publisher: American Association for the Advancement of Science) doi: 10.1126/science.abq2299

Wargan, K., Weir, B., Manney, G. L., Cohn, S. E., & Livesey, N. J. (2020). The anomalous 2019 Antarctic ozone hole in the GEOS constituent data assimilation system with MLS observations. *Journal of Geophysical Research: Atmospheres*, *125*(18), e2020JD033335. Retrieved from https://agupubs.onlinelibrary.wiley.com/doi/abs/10.1029/2020JD033335 (e2020JD033335 2020JD033335) doi: https://doi.org/10.1029/2020JD033335

WMO. (2023). *Scientific assessment of ozone depletion: 2022*. Geneva, Switzerland: Global Ozone Res. and Monit. Proj. Rep. 55.

Zhu, Y., Bardeen, C. G., Tilmes, S., Mills, M. J., Wang, X., Harvey, V. L., … Toon, O. B. (2022, October). Perturbations in stratospheric aerosol evolution due to the water-rich plume of the 2022 Hunga-Tonga eruption. *Communications Earth & Environment*, *3*(1), 1–7. Retrieved 2022-11-27, from https://www.nature.com/articles/s43247-022-00580-w (Number: 1 Publisher: Nature Publishing Group) doi: 10.1038/s43247-022-00580-w

Supporting Information for "Siege of the South: Hunga Tonga-Hunga Ha'apai Water Vapor Excluded from 2022 Antarctic Stratospheric Polar Vortex"

Gloria L. Manney[1,2], Michelle L. Santee[3], Alyn Lambert[3], Luis F. Millán[3], Ken Minschwaner[2], Frank Werner[3], Zachary D. Lawrence[4,5], William G. Read[3], Nathaniel J. Livesey[3], Tao Wang[3]

[1]NorthWest Research Associates, Socorro, NM, USA

[2]New Mexico Institute of Mining and Technology, Socorro, NM, USA

[3]Jet Propulsion Laboratory, California Institute of Technology, Pasadena, CA, USA

[4]Cooperative Institute for Research in Environmental Sciences (CIRES) & NOAA Physical Sciences Laboratory (PSL), University of Colorado, Boulder, Colorado, USA.

[5]NorthWest Research Associates, Boulder, CO, USA

Contents of this file

Corresponding author: Gloria L Manney, NorthWest Research Associates & New Mexico Institute of Mining and Technology, Department of Physics, 333 Workman, Socorro, NM 87801, USA. (manney@nwra.com)

Introduction

This file contains supplementary figures for "Siege of the South: Hunga Tonga-Hunga Ha'apai Water Vapor Excluded from 2022 Antarctic Stratospheric Polar Vortex".

Figures S1 and S2 show full-mission equivalent latitude (EqL) time series of the MLS fields shown in Figs. 1 and 2 in the main text, confirming the uniqueness of the extravortex HTHH signature in H_2O and the ordinariness of the evolution of all species within the stratospheric polar vortex. Fig. S3 presents Aura mission-long EqL/time plots at 380 K, showing only MLS species that have scientifically useful data at pressures of 215 hPa or above (since much of the 380 K surface is at pressures near or above that level), confirming that composition was not unusual in 2022 at subvortex levels. Figures S1 through S3 also include anomalies in two indicators of mixing, effective diffusivity (K_{eff}) and PV gradients. The years 2020 through 2022 all show relatively high PV gradient anomalies and low K_{eff} anomalies near the vortex edge in late winter and spring at all levels, consistent with the long-lived polar vortices in these years; other years during the Aura mission, including 2006, 2010, 2011, and 2015, show similar features, also generally related to long-lived polar vortices.

Figure S4 shows anomalies from the 2005–2021 climatology of vortex-averaged diabatic descent rates from MERRA-2 (note that stronger descent, that is, more negative values, is shown in red for emphasis), demonstrating that descent rates in the middle stratospheric vortex in late winter/early spring 2022 were smaller than usual (consistent, to first order, with lower vortex temperatures) but no more so than in several other years during the Aura mission. This is in contrast to large changes in descent in mid-latitudes (e.g., Coy et al., 2022).

Figures S5 through S7 show EqL/θ snapshots like those in Fig. 3 in the main text, but for 2018, 2020, and 2021 (a near-average year and two unusually cold years with larger-than-usual Antarctic "ozone holes"). Comparing these with Fig. 3 emphasizes that vortex conditions in 2022 were not extreme at any point during the season.

Figures S8 and S9 show profiles summarizing the evolution of dynamical diagnostics and trace gases presented in Fig. 4 in the main text. None of the vortex diagnostics (Fig. S8) show 2022 as the most extreme year in the 43-year MERRA-2 record at any level. Several of those maxima, especially related to vortex and polar processing potential duration, were redefined in 2020. 2021 also had an unusually strong and persistent lower stratospheric vortex, as did 2022, but there were previous years with stronger or more persistent vortices than each of these years. The MLS measurements (Fig. S9) emphasize clearly the near-average nature of the trace gas evolution in the vortex in 2022 from subvortex levels (the lower limit of the profiles shown is 370 K) to the upper stratosphere, consistent with the time series at selected levels shown in Fig. 4 in the main text. In particular, ClO was lower and lower-stratospheric O_3 higher in spring (October/November) 2022 than in 2020, 2021, and several other years also characterized by cold long-lived polar vortices.

As shown in Fig. 5 in the main text, scatter plots of H_2O with long-lived transport tracers demonstrate the separation of the HTHH enhancement from high H_2O that may descend inside the stratospheric polar vortex. Figure S10 shows the relationship between H_2O and CO in the middle stratosphere in the same way that Fig. 5 shows its relationship with N_2O. The results confirm the separation by the vortex edge transport barrier of air with high H_2O and low CO in the HTHH plume from air with high H_2O and high CO that descends inside the polar vortex.

Measurements from the Atmospheric Chemistry Experiment-Fourier Transform Spectrometer (ACE-FTS) also show the distinction between and separation from vortex air of the HTHH H_2O. Version 4.1/4.2 ACE-FTS data are used here, along with corresponding error flags (Boone et al., 2020; Sheese et al., 2022). Figure S11 shows mission-long ACE-FTS measurements of H_2O and the HDO / H_2O ratio (ΔD) at 700 and 550 K. The unprecedentedly high extravortex values of ΔD associated with the high H_2O demark the HTHH plume, since the seawater injected by HTHH has a higher isotope ratio (e.g., Randel et al., 2012; Khaykin et al., 2022, and references therein). ΔD generally increases with height and latitude in the stratosphere, similar to age of air (Randel et al., 2012), hence the larger values in the polar vortex. While ACE-FTS has coverage of much of the Antarctic polar vortex only in July–September, Figure S12 shows that during that time period, the high ΔD values in the HTHH plume are clearly separated from the high values in the polar vortex, with the latter generally occurring at lower H_2O values.

References

Boone, C., Bernath, P., Cok, D., Jones, S., & Steffen, J. (2020). Version 4 retrievals for the atmospheric chemistry experiment Fourier transform spectrometer (ACE-FTS) and imagers. *Journal of Quantitative Spectroscopy and Radiative Transfer*, *247*, 106939. Retrieved from https://www.sciencedirect.com/science/article/pii/S0022407319305916 doi: https://doi.org/10.1016/j.jqsrt.2020.106939

Coy, L., Newman, P. A., Wargan, K., Partyka, G., Strahan, S. E., & Pawson, S. (2022). Stratospheric Circulation Changes Associated With the Hunga Tonga-Hunga Ha'apai Eruption. *Geophysical Research Letters*, *49*(22), e2022GL100982. Retrieved 2022-11-27, from https://onlinelibrary.wiley.com/doi/abs/10.1029/2022GL100982 (_eprint: https://onlinelibrary.wiley.com/doi/pdf/10.1029/2022GL100982) doi: 10.1029/2022GL100982

Khaykin, S., Podglajen, A., Ploeger, F., Grooß, J.-U., Tence, F., Bekki, S., ... Ravetta, F. (2022, December). Global perturbation of stratospheric water and aerosol burden by Hunga eruption. *Communications Earth & Environment*, *3*(1), 316. Retrieved from https://doi.org/10.1038/s43247-022-00652-x

Randel, W. J., Moyer, E., Park, M., Jensen, E., Bernath, P., Walker, K., & Boone, C. (2012). Global variations of HDO and HDO/H2O ratios in the upper troposphere and lower stratosphere derived from ACE-FTS satellite measurements. *Journal of Geophysical Research: Atmospheres*, *117*(D6). Retrieved from https://agupubs.onlinelibrary.wiley.com/doi/abs/10.1029/2011JD016632 doi: https://doi.org/10.1029/2011JD016632

Sheese, P. E., Walker, K. A., Boone, C. D., Bourassa, A. E., Degenstein, D. A., Froidevaux, L., ... Zou, J. (2022). Assessment of the quality of ACE-FTS stratospheric ozone data. *Atmospheric Measurement Techniques*, *15*(5), 1233–1249. Retrieved from https://amt.copernicus.org/articles/15/1233/2022/ doi: 10.5194/amt-15-1233-2022

Figure S1. SH equivalent latitude / time series at 550 K of anomalies from the 2005–2021 climatology of (top to bottom) MERRA-2 effective diffusivity (K_{eff}) and sPV gradients and MLS temperature, N_2O, H_2O, HNO_3, HCl, ClO, and O_3, shown for the full Aura mission through January 2023. Black overlays are sPV contours indicating the vortex edge region.

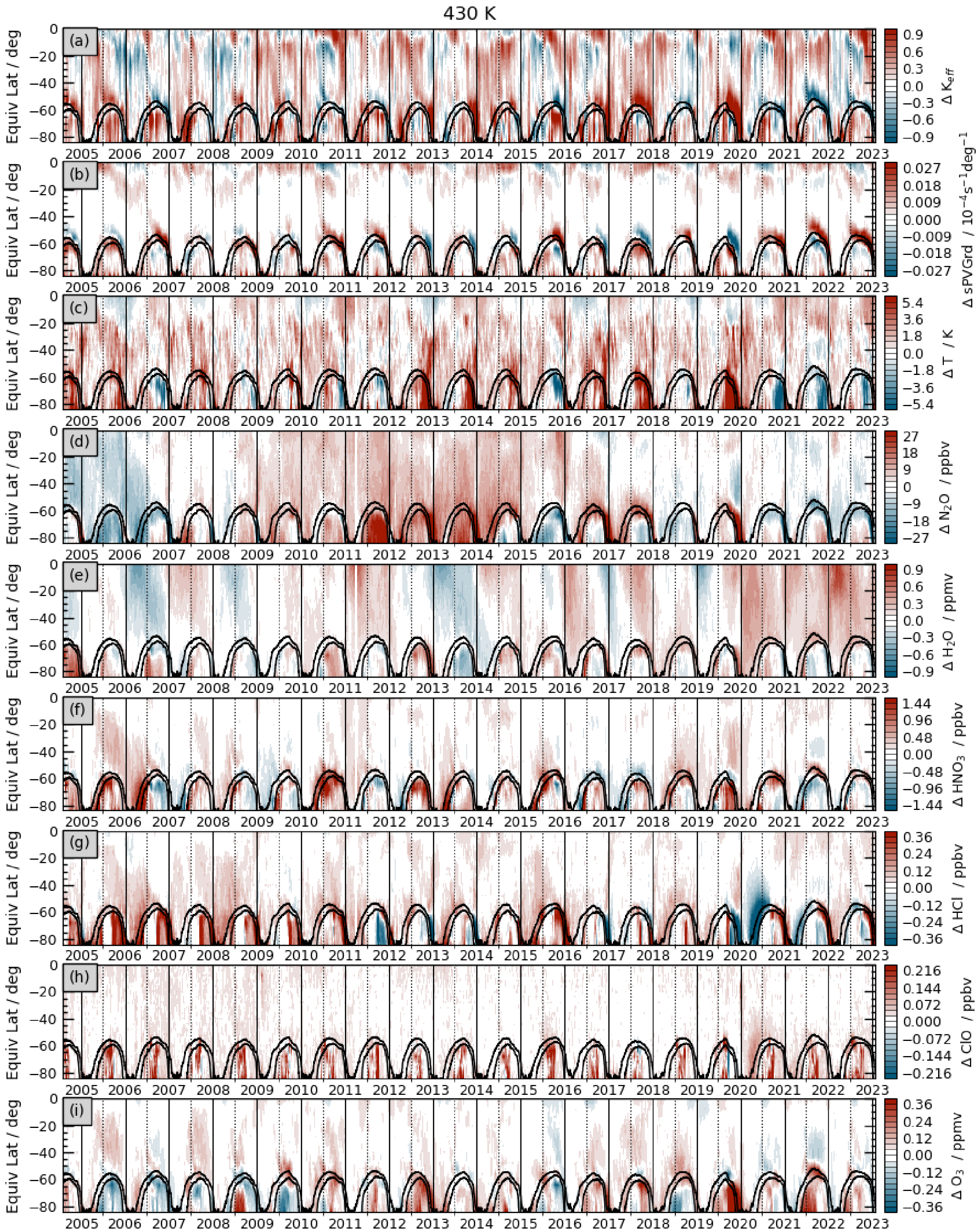

Figure S2. As in Fig. S1 but at 430 K.

Figure S3. As in Fig. S1, but for 380 K and showing only MLS species with scientifically useful data at 215 hPa and larger pressures.

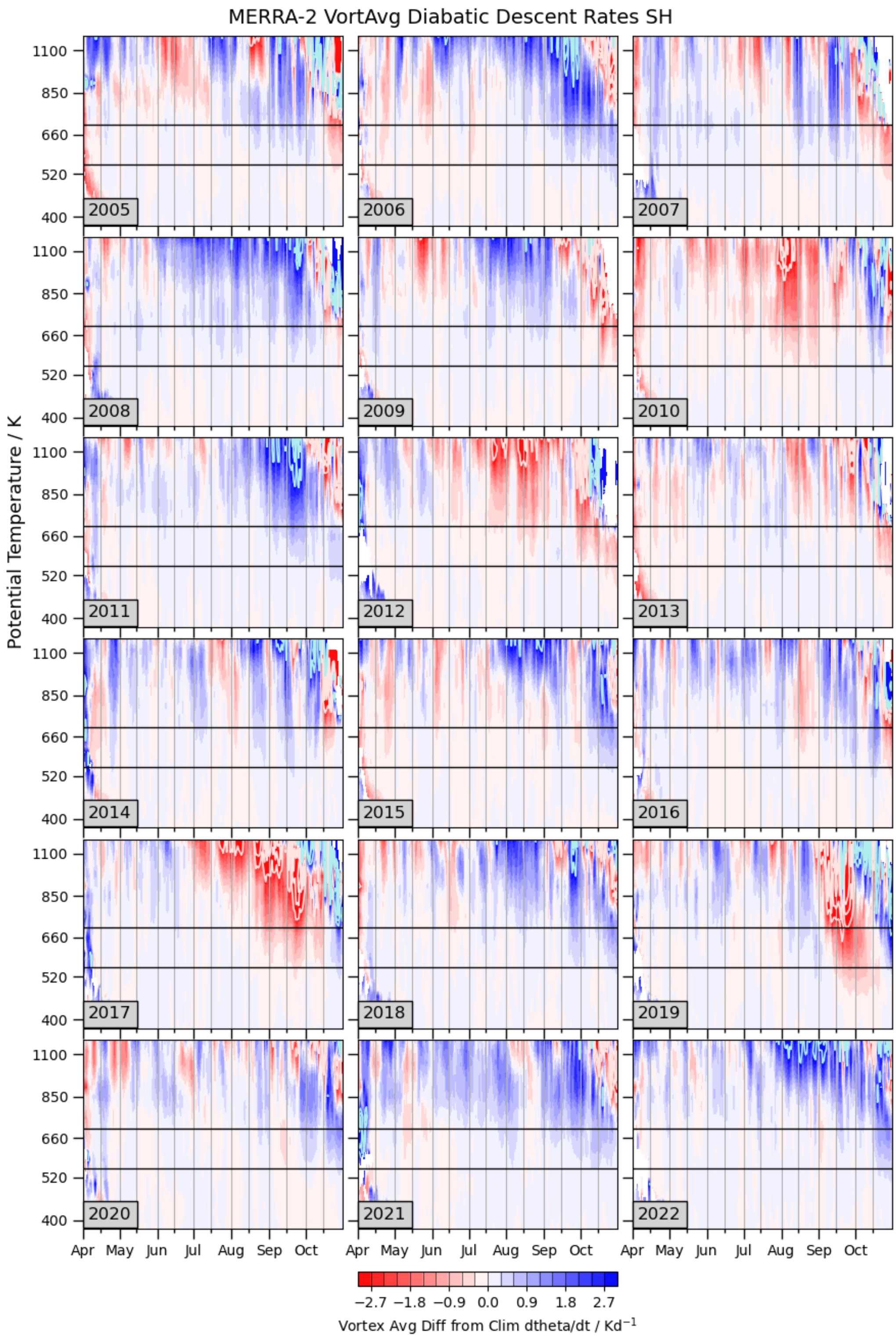

Figure S4. Cross-sections of anomalies from the 2005–2021 climatology of vortex-averaged diabatic heating/cooling rates from MERRA-2 for April through October in 2005 through 2022. Rates are expressed as dθ/dt. Up to three contours with an interval five times that shown in the colorbar are overlaid above the high value (cyan) and below the low value (pink) at which the color bar saturates. Overlaid horizontal lines mark 550 and 700 K. Note that the color scale has been inverted (negative values are reds) to emphasize anomalies indicating unusually strong descent.

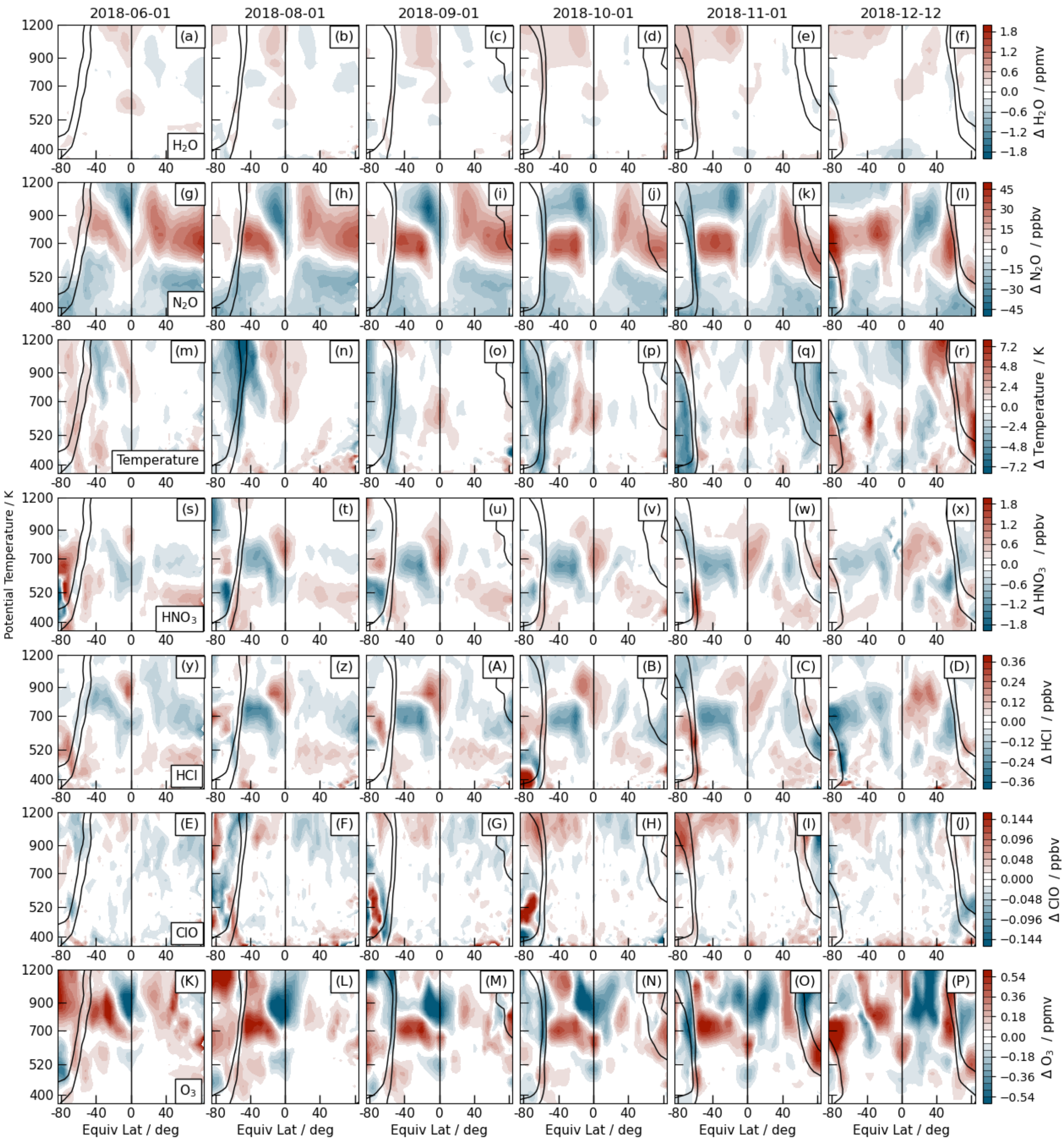

Figure S5. As in Fig. 3 in the main text, but for 2018: Snapshots on selected days in 2018 of anomalies from the 2005–2021 climatology of (top to bottom) MLS H_2O, N_2O, temperature, HNO_3, HCl, ClO, and O_3. Black overlaid contours are two contours of sPV representative of the vortex edge region.

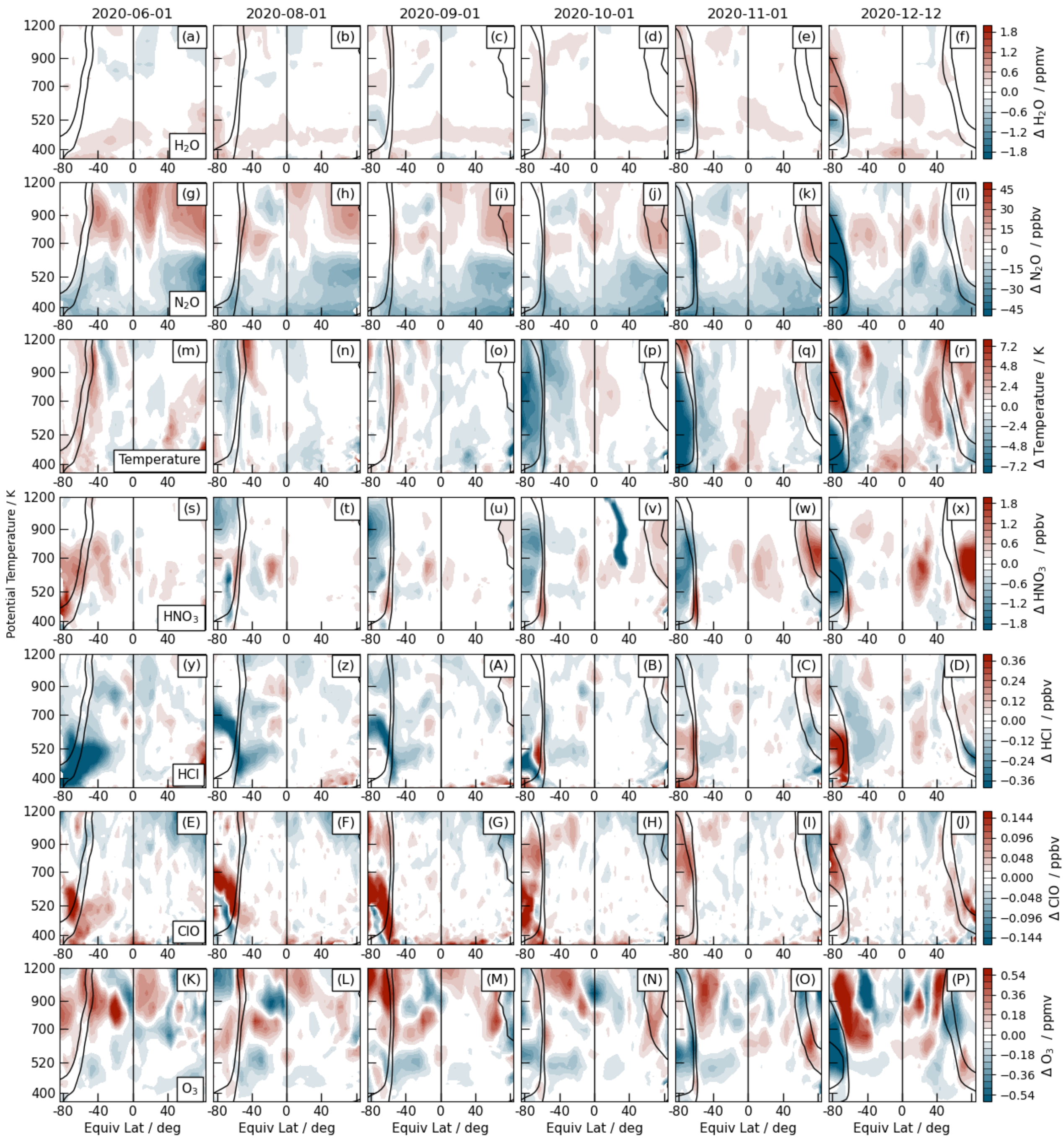

Figure S6. As in Fig. S5 but for 2020.

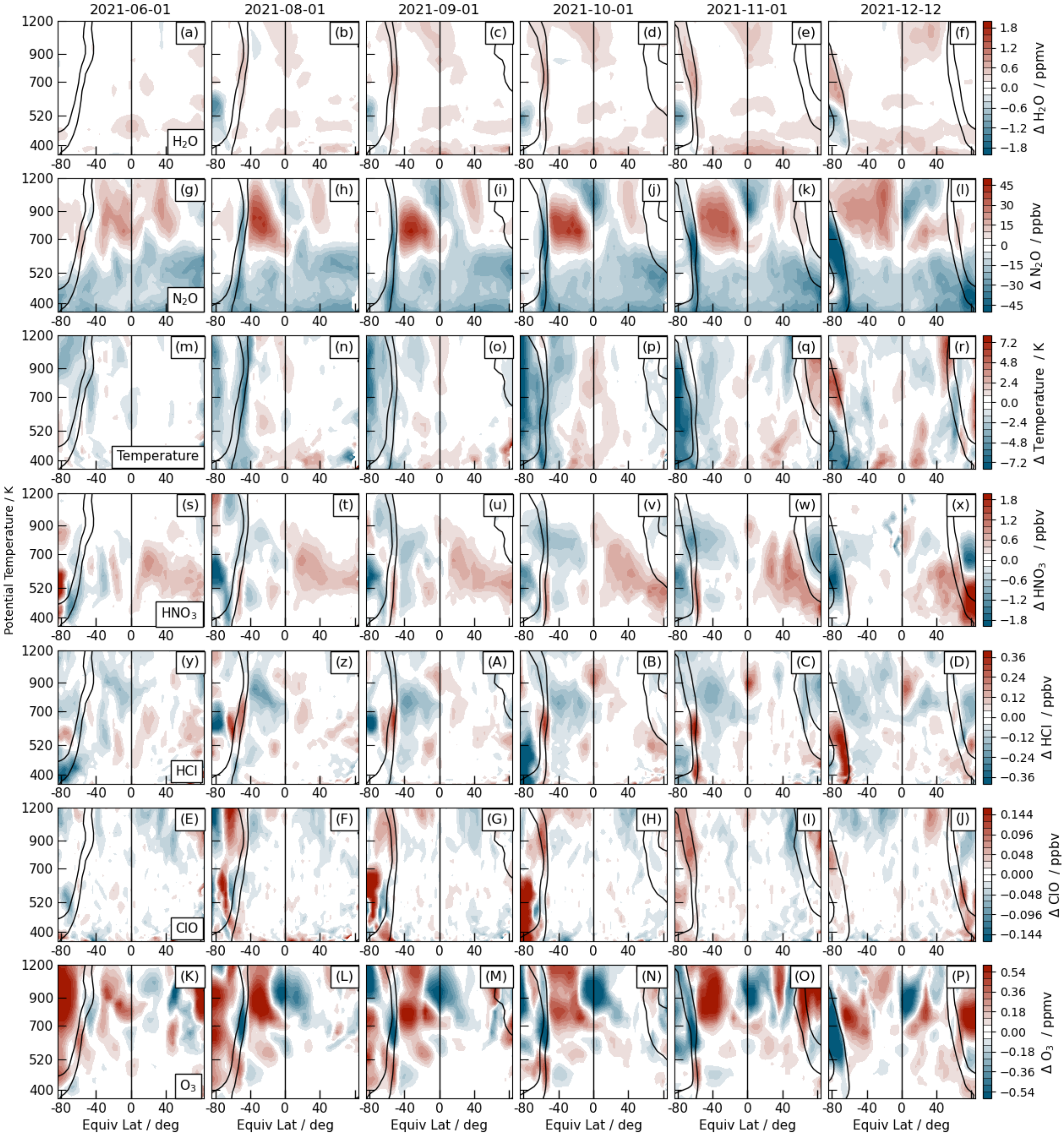

Figure S7. As in Fig. S5 but for 2021.

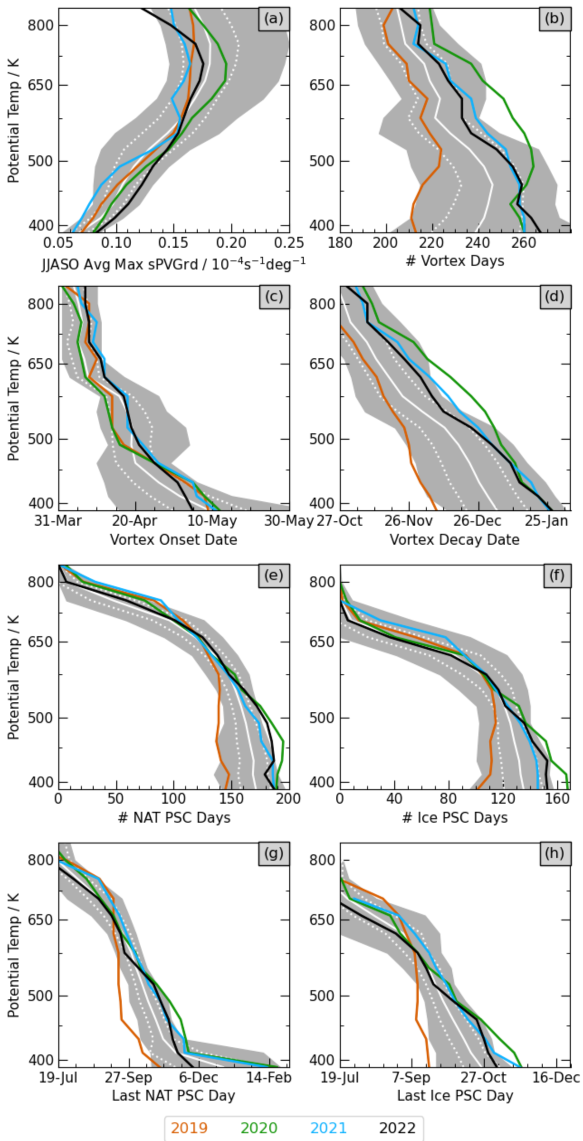

Figure S8. Profiles of summary vortex diagnostics calculated from MERRA-2 for 1979 through 2021 (excluding highlighted years). Highlighted years are 2019 (orange), 2020 (green), 2021 (cyan), and 2022 (black). Diagnostics are (left to right, top to bottom): June–October Average maximum sPV gradients; number of days when a vortex existed (defined as vortex area greater than 1% of a hemisphere); first date a vortex existed; last date a vortex existed; number of days with temperature less than the NAT PSC threshold; number of days with temperature less than the ice PSC threshold; last day temperatures were below the NAT PSC threshold; and last day temperatures were below the ice PSC threshold.

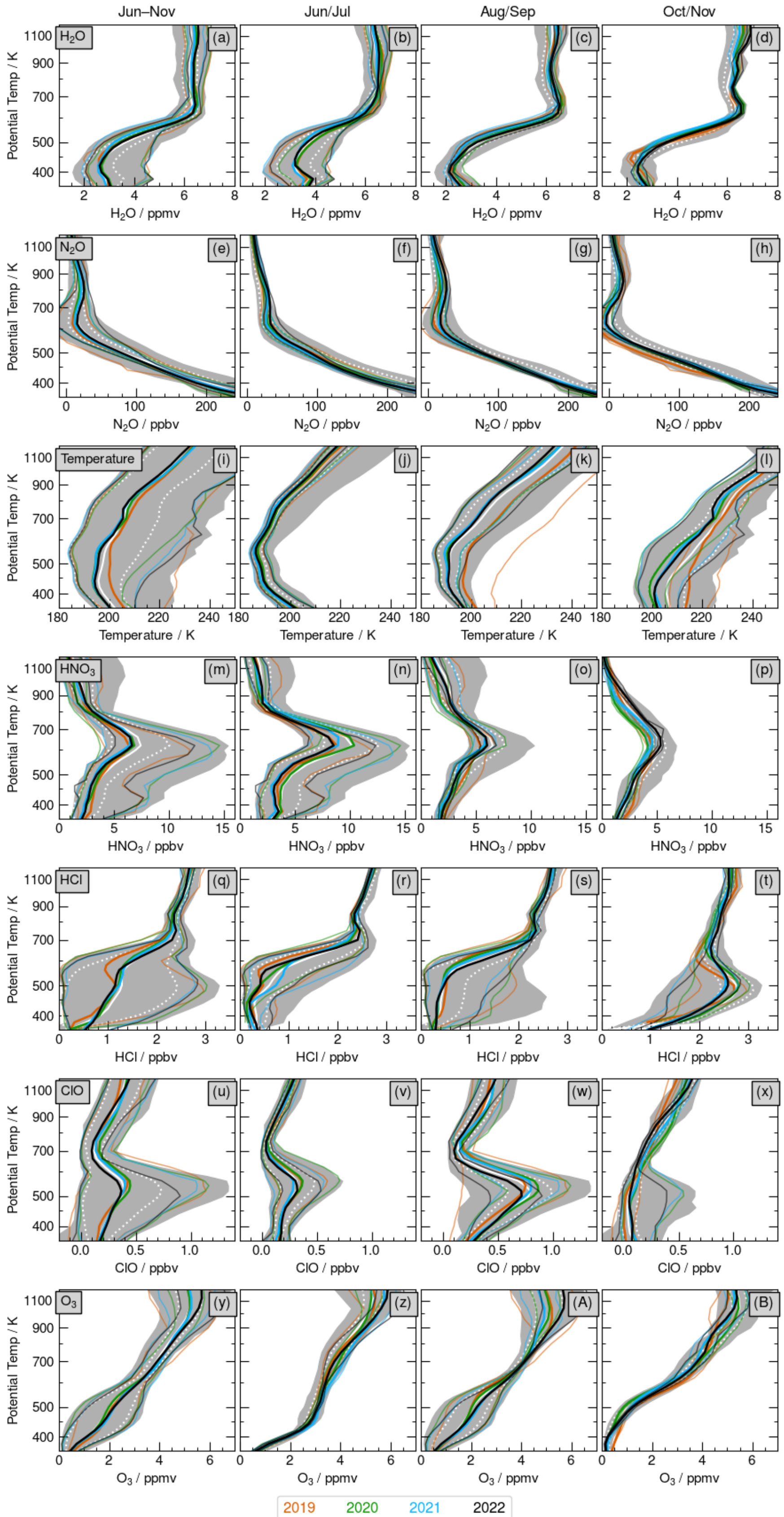

Figure S9. Profiles of vortex-averaged MLS data, averaged over (left to right) June through November; June/July; August/September; October/November. Fields shown are (top to bottom) H_2O, N_2O, temperature, HNO_3, HCl, ClO, and O_3. Grey envelope is the range excluding the highlighted years, and solid and dashed white lines are the mean and one standard deviation envelope for those years. Highlighted years are 2019 (orange), 2020 (green), 2021 (cyan), and 2022 (black).

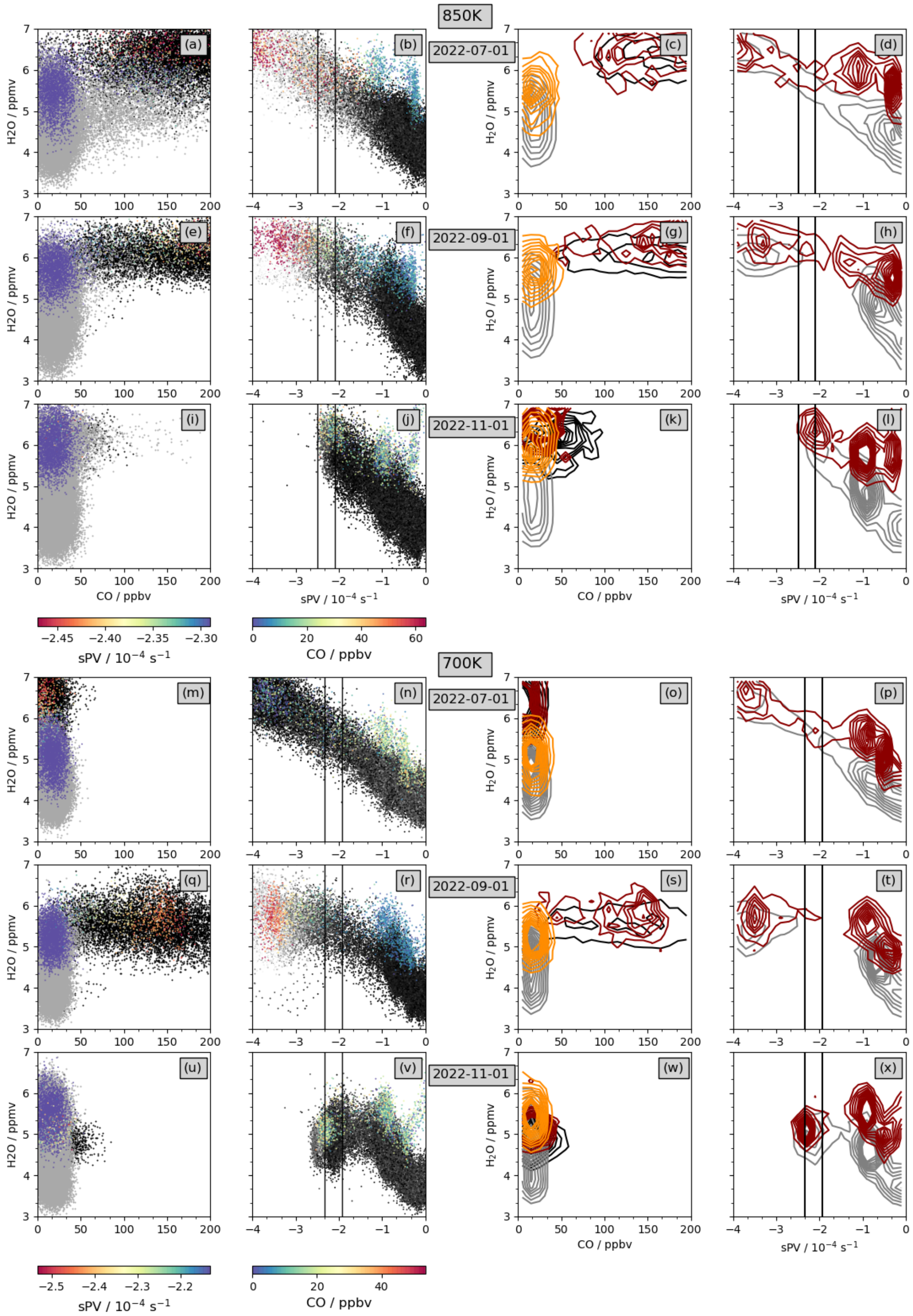

Figure S10. As in Fig. 5 in the main text, but for H_2O and sPV versus CO at 850 and 700 K: Scatter (left two columns) and density (right two columns) plots of MLS H_2O (y-axis) versus CO (first and third columns) and sPV (second and last columns). Grey and black dots (contours) show values from 2005–2021 in the scatter (density) plots; for those years, black (grey) indicates x-axis values of CO or sPV characteristic of inside (outside) the vortex. For 2022, colored (purple) dots or dark red (orange) contours show sPV values inside (outside) the vortex. 2022 CO (second column) is colored such that blue/blue-green shows typical vortex values. Black vertical lines on the plots versus sPV indicate the vortex edge region.

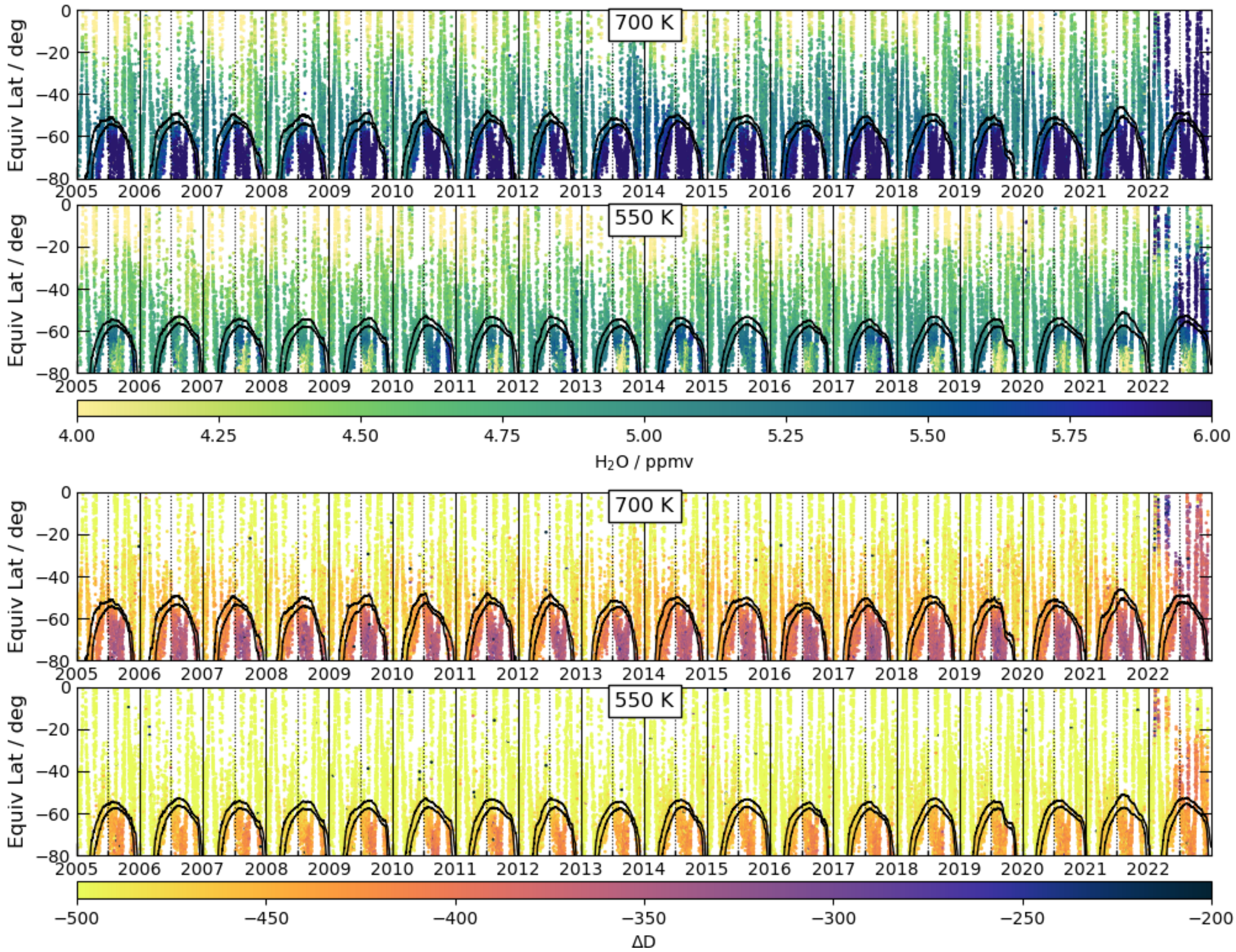

Figure S11. 700 and 550 K EqL/time plots of ACE-FTS H_2O and ΔD (HDO/H_2O, scaled as in Randel et al., 2012) for 2005–2022. Black overlays are sPV contours in the vortex edge region.

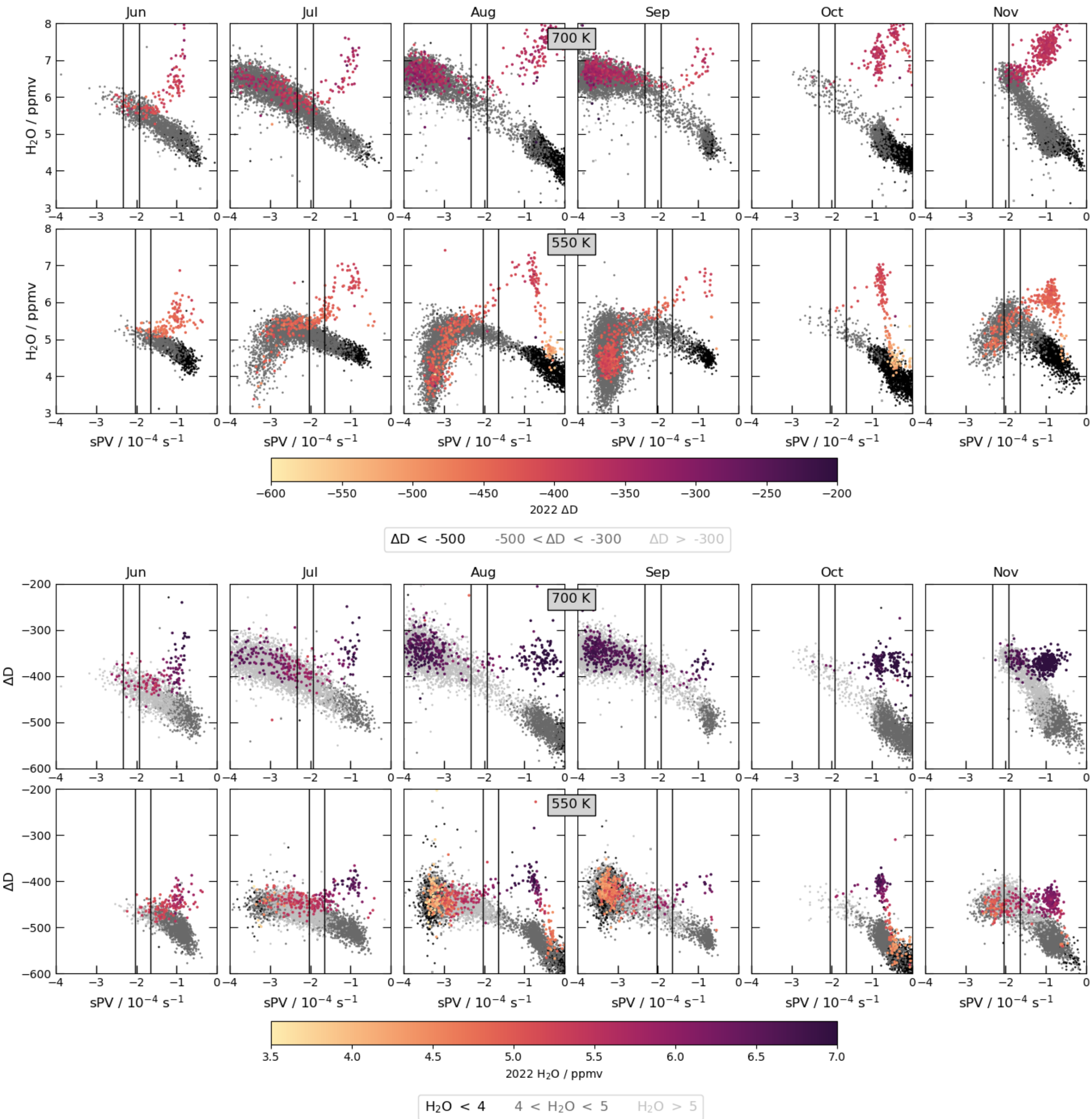

Figure S12. ACE-FTS H_2O and ΔD as a function of sPV, with 2022 values colored by ΔD and H_2O, respectively, and high, medium, and low values shown in black, grey, and pale grey, respectively, for preceding years from 2005 through 2021.